Cell

In vivo CRISPR screens identify the E3 ligase *Cop1* as a modulator of macrophage infiltration and cancer immunotherapy target

Graphical abstract

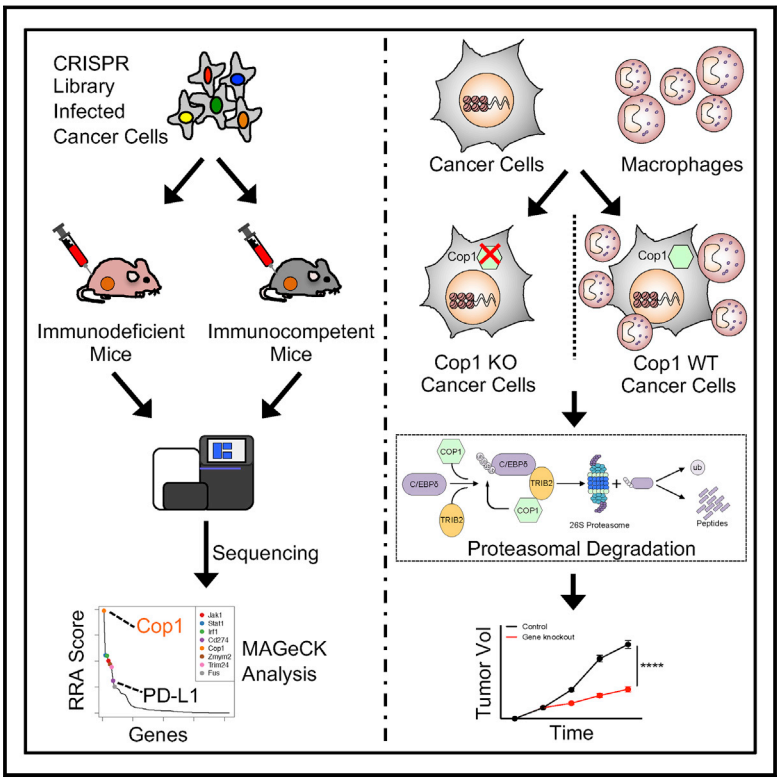

Highlights

- *In vivo* CRISPR screens identify new immune targets regulating the tumor microenvironment
- Cop1 knockout in cancer cells enhances anti-tumor immunity
- Cop1 modulates chemokine secretion and macrophage infiltration into tumors
- Cop1 targets C/ebpδ degradation via Trib2 and influences ICB response

Authors

Xiaoqing Wang, Collin Tokheim, Shengqing Stan Gu, ..., Henry Long, Myles Brown, X. Shirley Liu

Correspondence

myles_brown@dfci.harvard.edu (M.B.), xsliu@ds.dfci.harvard.edu (X.S.L.)

In brief

Large-scale *in vivo* CRISPR screens reveal that *Cop1* knockout in cancer cells stabilizes *C/ebpδ* protein, suppressing macrophage infiltration and enhancing anti-tumor immunity.

Wang et al., 2021, Cell *184*, 1–18
October 14, 2021 © 2021 Elsevier Inc.
https://doi.org/10.1016/j.cell.2021.09.006

CellPress

Please cite this article in press as: Wang et al., *In vivo* CRISPR screens identify the E3 ligase *Cop1* as a modulator of macrophage infiltration and cancer immunotherapy target, Cell (2021), https://doi.org/10.1016/j.cell.2021.09.006

Cell

CellPress

Article

In vivo CRISPR screens identify the E3 ligase *Cop1* as a modulator of macrophage infiltration and cancer immunotherapy target

Xiaoqing Wang,[1,2,3,4,6,12] Collin Tokheim,[2,3,4,12] Shengqing Stan Gu,[1,2,3,4,12] Binbin Wang,[2,3,7,12] Qin Tang,[1,2,4,8] Yihao Li,[1,4] Nicole Traugh,[2,9] Zexian Zeng,[2,3,4] Yi Zhang,[2,3,4] Ziyi Li,[2] Boning Zhang,[1,2,3,4] Jingxin Fu,[1,2] Tengfei Xiao,[1,2,3,4,10] Wei Li,[2,3,4,11] Clifford A. Meyer,[2,3,4] Jun Chu,[2,5] Peng Jiang,[2,3,4,7] Paloma Cejas,[4] Klothilda Lim,[4] Henry Long,[4] Myles Brown,[1,4,*] and X. Shirley Liu[2,3,4,13,*]

[1]Department of Medical Oncology, Dana-Farber Cancer Institute, Boston, MA 02215, USA
[2]Department of Data Science, Dana-Farber Cancer Institute, Boston, MA 02215, USA
[3]Department of Biostatistics, Harvard T.H. Chan School of Public Health, Boston, MA 02215, USA
[4]Center for Functional Cancer Epigenetics, Dana-Farber Cancer Institute, Boston, MA 02215, USA
[5]Key Laboratory of Xin'an Medicine, Ministry of Education, Anhui University of Chinese Medicine, Hefei, Anhui 230038, China
[6]Present address: Department of Cardiology, Shanghai Jiao Tong University Affiliated Sixth People's Hospital, Shanghai 200233, China
[7]Present address: Center for Cancer Research, National Cancer Institute, Bethesda, MD 20892, USA
[8]Present address: Salk Institute for Biological Studies, San Diego, CA 92037, USA
[9]Present address: Graduate School of Biomedical Sciences, Tufts University, Boston, MA 02111, USA
[10]Present address: GV20 Oncotherapy, Shanghai 201203, China
[11]Present address: Center for Genetic Medicine Research, Children's National Hospital. Washington DC 20010, USA
[12]These authors contributed equally
[13]Lead contact
*Correspondence: myles_brown@dfci.harvard.edu (M.B.), xsliu@ds.dfci.harvard.edu (X.S.L.)
https://doi.org/10.1016/j.cell.2021.09.006

SUMMARY

Despite remarkable clinical efficacy of immune checkpoint blockade (ICB) in cancer treatment, ICB benefits for triple-negative breast cancer (TNBC) remain limited. Through pooled *in vivo* CRISPR knockout (KO) screens in syngeneic TNBC mouse models, we found that deletion of the E3 ubiquitin ligase *Cop1* in cancer cells decreases secretion of macrophage-associated chemokines, reduces tumor macrophage infiltration, enhances anti-tumor immunity, and strengthens ICB response. Transcriptomics, epigenomics, and proteomics analyses revealed that *Cop1* functions through proteasomal degradation of the *C/ebpδ* protein. The *Cop1* substrate *Trib2* functions as a scaffold linking *Cop1* and *C/ebpδ*, which leads to polyubiquitination of *C/ebpδ*. In addition, deletion of the E3 ubiquitin ligase *Cop1* in cancer cells stabilizes *C/ebpδ* to suppress expression of macrophage chemoattractant genes. Our integrated approach implicates *Cop1* as a target for improving cancer immunotherapy efficacy in TNBC by regulating chemokine secretion and macrophage infiltration in the tumor microenvironment.

INTRODUCTION

Breast cancer is one of the leading causes of cancer-associated morbidity and mortality in the United States (Fallahpour et al., 2017; Waks and Winer, 2019). Triple-negative breast cancer (TNBC) constitutes 15% of breast cancer cases and has the worst prognosis among the molecular subtypes, motivating research efforts to find new treatment options (Bianchini et al., 2016). Immune checkpoint blockade (ICB) has shown remarkable clinical benefits for individuals with skin, lung, and colorectal cancer (Halle et al., 2017), raising the possibility of effective ICB treatment of breast cancer. In 2019, the US Food and Drug Administration approved the first ICB therapy for treatment of metastatic TNBC. Atezolizumab, an anti-PD-L1 monoclonal antibody, was approved in combination with nab-paclitaxel (nanoparticle albumin-bound paclitaxel) based on prolonged progression-free survival (Schmid et al., 2018). Although this advance demonstrates the promise of ICB in breast cancer treatment, the benefits were limited to a small subset of individuals. A recent clinical trial reported that pembrolizumab, an anti-PD-1 monoclonal antibody, had an objective response rate of just 18% in PD-L1-expressing advanced TNBC (Nanda et al., 2016). This underscores the need for finding new immune targets to enhance ICB response and improve outcomes in TNBC.

The immune system is known to play important roles in cancer progression (Coussens et al., 2013; Hanahan and Weinberg, 2011), although the molecular mechanisms regulating tumor immunity and the tumor microenvironment (TME) are not fully

Please cite this article in press as: Wang et al., *In vivo* CRISPR screens identify the E3 ligase *Cop1* as a modulator of macrophage infiltration and cancer immunotherapy target, Cell (2021), https://doi.org/10.1016/j.cell.2021.09.006

understood. Some cell types in the TME are proposed to promote tumor growth and metastasis, such as myeloid-derived suppressor cells (MDSCs) (Grivennikov et al., 2010), fibroblasts (Landskron et al., 2014), and tumor-associated macrophages (TAMs) (Su et al., 2018). Among them, TAMs are major players and are thought to promote angiogenesis, cancer cell local invasion, and intravasation at primary tumor sites. At metastatic sites, TAMs can also facilitate cancer cell extravasation and block $CD8^+$ T cell recruitment and functions (Cassetta and Pollard, 2018; Peranzoni et al., 2018). In affected individuals, macrophage infiltration in tumors is strongly associated with poor clinical outcome in numerous cancer types, including breast cancer (Cassetta et al., 2019; Zhang et al., 2016). In syngeneic mouse models, classical monocytes (mouse $CD11b^+Ly6C^+$) are recruited to tumors and differentiate into TAMs as tumors progress (Ginhoux and Jung, 2014). This process often depends on macrophage chemoattractants secreted from cancer cells or activated macrophages, such as CCL2 (Nielsen and Schmid, 2017), CCL4 (Li et al., 2018), CCL5 (Walens et al., 2019), CXCL1 (Wang et al., 2017), and CXCL5 (Zhao et al., 2017). Accordingly, a monoclonal antibody was developed to inhibit the CCL2 signaling pathway, which indeed attenuates TAM infiltration, suppresses tumor growth, and improves survival (Qian et al., 2011). However, pharmacological inhibition of chemokines is associated with chemokine overexpression because of homeostatic feedback, yielding adverse effects (Lim et al., 2016). These findings motivated us to discover novel targets to reprogram the TME for cancer treatment.

Functional genomic screening using CRISPR-Cas9 has shown promise as a robust and unbiased approach to discover novel cancer targets. It has also been adopted to find novel modulators of tumor immunity, discover novel immuno-oncology targets, and dissect their mechanisms. For instance, fluorescence-activated cell sorting (FACS)-based genome-wide CRISPR screens *in vitro* have discovered multiple regulators of PD-L1 and/or major histocompatibility complex (MHC) class I, which potentially facilitate combination immunotherapies for cancer (Burr et al., 2017; Dersh et al., 2021; Gu et al., 2021; Mezzadra et al., 2017). CRISPR screens in cancer cells co-cultured with T cells identified *Pbrm1* loss as increasing the sensitivity of B16F10 melanoma cells to effector T cells (Pan et al., 2018). A separate screen in cancer cells co-cultured with T cells identified genes that, when knocked out in cancer cells, induce immune escape (Lawson et al., 2020). Pooled *in vivo* CRISPR screens in murine melanoma models revealed that loss of *Ptpn2* (Manguso et al., 2017) and *Adar1* (Ishizuka et al., 2019) could enhance tumor sensitivity to immunotherapy. Although *in vivo* CRISPR screens effectively query broad aspects of tumor immunity, only a few hundred genes at a time can be screened. This has limited their application to a restricted set of tumor models. This encouraged us to test more genes in different syngeneic models using *in vivo* CRISPR screens with the intention of identifying new regulators of tumor immunity.

In this study, we constructed custom murine CRISPR knockout libraries and used them to conduct *in vivo* CRISPR screens in murine TNBC and colon cancer models under different levels of host immunity. Through two rounds of *in vivo* screens, we identified the E3 ubiquitin ligase *Cop1* as an important regulator of tumor-infiltrating M2 macrophages and anti-PD-1 response *in vivo*. To further characterize the function and mechanisms of *Cop1* in cancer cells, we performed detailed RNA sequencing (RNA-seq), ATAC-seq, and proteomics analyses to identify *Cop1*'s substrate. Deletion of *Cop1* in TNBC cells led to increased *C/ebpδ* protein stability and chromatin binding, which suppresses expression of key macrophage chemoattractants and cytokines involved in macrophage chemotaxis and activation. Detailed analysis of the substrates that were altered significantly upon *Cop1* depletion revealed that *Cop1* targets *C/ebpδ* for proteasome degradation via the scaffolding protein *Trib2*. Observations of clinical tumor immune infiltration and survival of affected individuals across many cancer types strongly support the clinical relevance of *Cop1* as a tumor-immune modulator of *C/ebpδ*-regulated macrophage infiltration. More generally, our study demonstrates the power of systems biology approaches in identifying modulators of macrophage infiltration and cancer immunotherapy targets.

RESULTS

Large-scale *in vivo* CRISPR screens identify regulators of immune evasion

To systematically discover gene targets in cancer cells whose loss enhances anti-tumor immunity, we first constructed a murine lentiviral CRISPR-Cas9 knockout (MusCK) library. This library includes 5 sgRNAs for each of over 4,500 genes implicated in tumor initiation, progression, and immune modulation (Figure S1A; Table S1; see STAR Methods for further details). To validate the quality of the MusCK library, we transduced it into the mouse TNBC cell line 4T1 *in vitro* (Figure S1B; see STAR Methods for further details). 4T1 cells closely resemble human TNBC cells (Figures S1C and S1D), are transplantable into syngeneic BALB/c background mice, and have been used extensively in tumor immunology studies (Kim et al., 2014; Sagiv-Barfi et al., 2015). We compared sgRNA abundance distributions in freshly infected 4T1 cells with those in 4T1 cells cultured 10 passages after infection. Supporting the reliability of the MusCK library, cells harboring sgRNAs targeting known oncogenes and tumor suppressor genes were significantly depleted and enriched, respectively (Figures S1E and S1F; Table S2).

With the MusCK library validated, we next conducted *in vivo* CRISPR screens in 4T1 cells in syngeneic BALB/c mice. To this end, we first artificially expressed membrane-bound ovalbumin (mOva) in 4T1 cells, an approach used widely to enhance cellular immune responses in syngeneic tumor models. As expected, 4T1 tumors overexpressing mOva had increased lymphocyte infiltration and slower tumor growth (Figures S1G–S1J; see STAR Methods for further details). We then transduced the lentiviral MusCK library into mOva-expressing 4T1 cells and implanted infected cells into the mammary fat pads of BALB/c $Foxn1^{nu/nu}$ hosts (nude), immune competent BALB/c hosts, and BALB/c hosts vaccinated with ovalbumin prior to transplantation (Figure 1A; Figures S1K and S1L). We used 12 mice per arm and injected enough cells per mouse to achieve ~200-fold coverage for all sgRNAs in the MusCK library. Sixteen days after transplantation, we harvested the engrafted cancer cells for analysis and observed significantly different tumor growth in

Please cite this article in press as: Wang et al., *In vivo* CRISPR screens identify the E3 ligase *Cop1* as a modulator of macrophage infiltration and cancer immunotherapy target, Cell (2021), https://doi.org/10.1016/j.cell.2021.09.006

CellPress

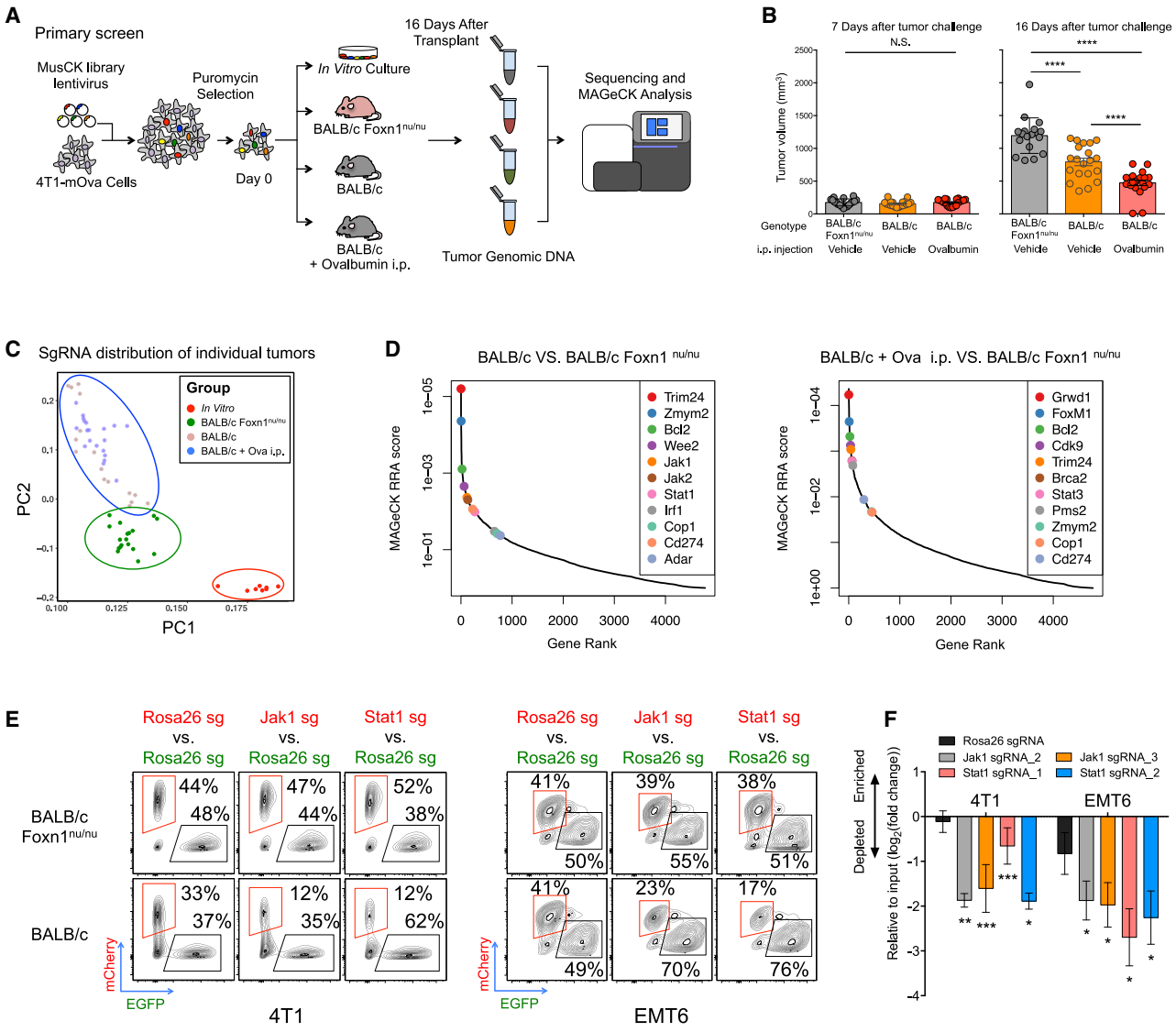

Figure 1. *In vivo* screens with the MusCK library uncover classic and novel regulators of immune evasion

(A) Workflow of MusCK *in vivo* screens to identify the potential targets for immune evasion. i.p., intraperitoneal.

(B) Tumor volume measured 7 and 16 days after implantation in the MusCK screens. Data are shown as mean ± SEM; n = 10–12 mice per group; ****p < 0.0001 by one-way ANOVA with Benjamini-Hochberg multiple test correction.

(C) Principal-component analysis of sgRNA abundance under each condition of the MusCK screens.

(D) Top depleted genes in immunocompetent versus immunodeficient (nude) hosts in the MusCK screens.

(E) Flow cytometry analysis of Jak1 (or *Stat1*) KO cells versus control *Rosa26* KO mouse breast cancer cells in the resulting 4T1 and EMT6 tumors.

(F) Quantification of relative percentages calculated from flow cytometry analysis. Data are shown as mean ± SEM; n = 4–6 mice per group; *p < 0.05, **p < 0.01, ***p < 0.001 by one-way ANOVA with Benjamini-Hochberg multiple test correction.

different hosts. T cell-deficient BALB/c Foxn1$^{nu/nu}$ hosts had the biggest tumors, and immune-competent hosts pre-vaccinated with ovalbumin had the smallest tumors (Figure 1B; Figure S1M).

To analyze the CRISPR screen results, we examined the sgRNA abundance distribution in the resulting 4T1 tumors grown *in vivo*. Reflective of different selection pressure in the hosts, principal-component analysis showed that CRISPR screen samples separated first by *in vitro* versus *in vivo* conditions and then by nude mice versus immunocompetent mice (Figure 1C). Samples from the same condition cluster together, indicating similar library representations in biological replicates (Figure 1C). Inspection of the sgRNAs depleted from tumors in wild-type immunocompetent hosts compared with nude immunodeficient mice revealed key genes promoting immune evasion in 4T1 cancer cells (Figure 1D; Table S3; see STAR Methods for further details). As positive controls, sgRNAs targeting *Cd274* (*Pd-l1*) were depleted in tumors engrafted in wild-type mice, consistent with the known function of *Cd274* in immune suppression (Dong

Please cite this article in press as: Wang et al., *In vivo* CRISPR screens identify the E3 ligase *Cop1* as a modulator of macrophage infiltration and cancer immunotherapy target, Cell (2021), https://doi.org/10.1016/j.cell.2021.09.006

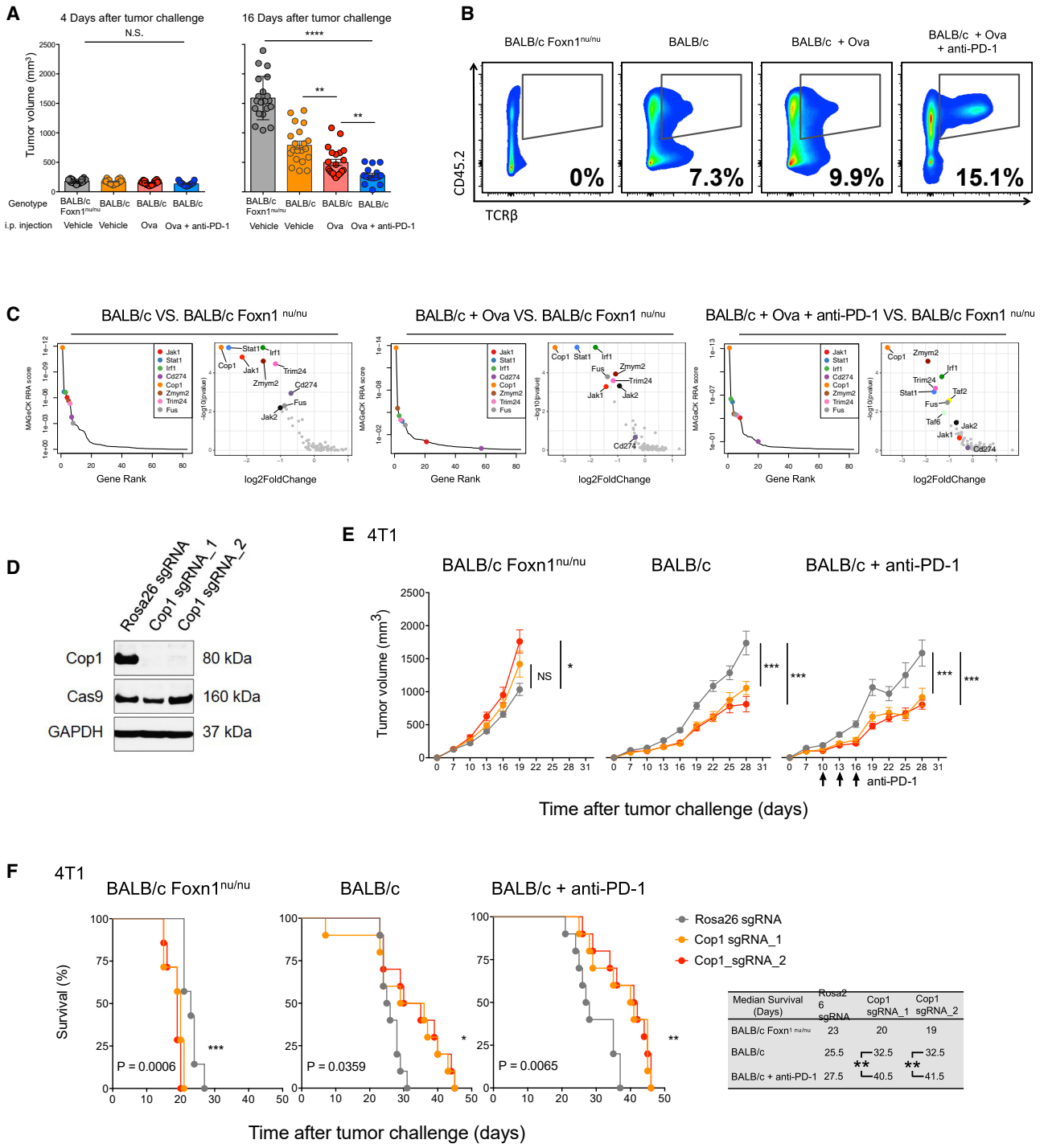

Median Survival (Days)	Rosa26 sgRNA	Cop1 sgRNA_1	Cop1 sgRNA_2
BALB/c Foxn1 nu/nu	23	20	19
BALB/c	25.5	32.5	32.5
BALB/c + anti-PD-1	27.5	40.5	41.5

Figure 2. Second-round MusCK screens identify *Cop1* as a regulator of TNBC progression

(A) Tumor volume measured 4 and 16 days after implantation in the MusCK 2.0 screens. Data are shown as mean ± SEM; n = 7–12 mice per group; **p < 0.01, ****p < 0.0001 by one-way ANOVA with Benjamini-Hochberg multiple test correction.

(B) Flow cytometry analysis of the tumor-infiltrating T cell population (TCRβ+) among the total immune cell population (Cd45.2+).

(C) MAGeCK analysis and RRA ranking of top depleted genes in the MusCK 2.0 screens. Ranked dot plots of depleted genes in immunocompetent hosts compared with immunodeficient nude hosts are shown.

(D) Western blot of *Cop1* protein level in 4T1 mouse TNBC cells transduced with sgRNA targeting *Cop1* and *Rosa26*.

(legend continued on next page)

Please cite this article in press as: Wang et al., *In vivo* CRISPR screens identify the E3 ligase *Cop1* as a modulator of macrophage infiltration and cancer immunotherapy target, Cell (2021), https://doi.org/10.1016/j.cell.2021.09.006

et al., 1999; Freeman et al., 2000). In addition, key components of DNA repair pathways, such as *Brca2* and *Pms2*, were significantly negatively selected in wild-type mice (Figure 1D). This is also consistent with previous reports that cancer cells with greater genome instability or mutation burden were at risk of elimination by T cell-mediated killing (Mandal et al., 2019; Pearlman et al., 2017).

Interestingly, key components of the interferon γ (IFNγ) pathway (*Jak1*, *Jak2*, *Stat1*, and *Irf1*) were significantly depleted in wild-type mice but not nude mice (Figure 1D), suggesting that defects in the IFNγ pathway in cancer cells could suppress immune evasion. IFNγ is a cytokine secreted by tumor-infiltrating lymphocytes to elicit an anti-tumor immune response (Alshaker and Matalka, 2011). This result is contrary to previously reported findings from CRISPR-mediated genetic knockout (KO) screens in the murine B16F10 melanoma model (Manguso et al., 2017) but consistent with the role of IFNγ in promoting tumor immune evasion in multiple cancer types (Beatty and Paterson, 2000; Benci et al., 2016, 2019). There have been reports that the duration of IFNγ signaling contributes to differential tumor responses to ICB, which may explain this apparent discrepancy (Minn, 2015). RNA-seq analysis revealed that IFNγ signaling was active in 4T1 tumors *in vivo* but not in 4T1 cells *in vitro* (Figure S1N). Thus, it is possible that prolonged IFNγ signaling in tumors has an immunosuppressive function, which would explain why KO of IFNγ pathway genes enhances immune-mediated killing of TNBC cells.

To confirm our findings, we conducted a competition assay to assess the *in vivo* growth of 4T1 TNBC cells deficient in IFNγ signaling (Figure S1O). Western blotting confirmed the protein abundance of *Jak1* or *Stat1* KO in TNBC cells (Figure S1P). Then we mixed cancer cells (1:1 ratio, mCherry:EGFP) with *Jak1* (or *Stat1*) KO and control *Rosa26* KO cells (see STAR Methods for further details) and implanted the cell mixture into nude and wild-type mice. Flow cytometry analysis of the resulting tumors showed that the relative proportion of *Jak1* or *Stat1* KO cancer cells became consistently and significantly lower than those of control cells (Figures 1E and 1F), especially in wild-type mice. The same result was observed in another TNBC syngeneic model, EMT6 (Figures 1E and 1F), which not only supports the reliability of *in vivo* screens using our MusCK library but also confirms the role of IFNγ signaling in suppressing an anti-tumor immune response in TNBC.

Loss of *Cop1* sensitizes cancers to immunotherapy

Achieving adequate statistical significance for discovery in large-scale CRISPR screens requires behavioral consistency of multiple sgRNAs, each with sufficient cell coverage, for each target gene, especially under negative selection. To improve the robustness of our *in vivo* CRISPR screens, we constructed a second library (MusCK 2.0) focused on 79 candidate genes identified in the primary screen, with 8 sgRNAs per gene (see STAR Methods for further details). We then conducted a validation screen using the MusCK 2.0 library in 4T1-mOva cells implanted into (1) BALB/c Foxn1$^{nu/nu}$ nude hosts, (2) wild-type BALB/c hosts, (3) wild-type BALB/c hosts with ovalbumin pre-vaccination, and (4) wild-type BALB/c hosts with ovalbumin pre-vaccination and monoclonal anti-PD-1 treatment (Figure S2A). The fourth group facilitates discovery of factors that affect antigen-specific T cell immunity through the PD-1/PD-L1 axis. As expected, we observed statistically significant and progressively lower tumor volumes in groups 1–4 16 days after cancer cell implantation (Figure 2A; Figures S2A–S2C). We also observed progressively higher T cell infiltration (detected by TCRβ^{+}) relative to the total tumor immune infiltrates (marked by Cd45.2^{+}) (Figure 2B; Figures S2D–S2F) in these four groups. In wild-type BALB/c hosts (groups 2–4) relative to Foxn1$^{nu/nu}$ hosts, one would expect depletion of genes required for an effective immune response. Indeed, we observed significant depletion of known mediators of immune evasion (*Cd274*/*Pd-l1*) and components of the IFNγ signaling pathway (*Jak1*, *Jak2*, *Stat1*, and *Irf1)*. We also observed depletion of an oncogenic transcriptional activator identified previously by our laboratory in prostate cancer (*Trim24)* (Groner et al., 2016), an E3 ubiquitin ligase (*Cop1*), and others (Figure 2C; Table S4). The phenotypes of these genes in 4T1 tumors were also observed in a second murine TNBC model (EMT6) (Figures S2G–S2J) and a murine colorectal cancer model (MC38) (Figures S3A–S3D), validating the robustness of our findings.

After two rounds of *in vivo* screens, *Cop1* emerged as the most significantly depleted gene in 4T1 tumors from immunocompetent mice relative to nude mice (Figures S3E and S3F). Although *Cop1* KO cells did not decrease viability compared with control *Rosa26* KO cells *in vitro* (Figure 2D; Figure S3G), we observed significantly slower tumor progression of *Cop1* KO TNBC cells *in vivo* in wild-type BALB/c hosts with and without anti-PD-1 treatment (Figure 2E; Figure S3H). Kaplan-Meier survival analysis showed that wild-type mice with *Cop1*-deficient tumors had prolonged survival with or without anti-PD-1 treatment compared with nude mice (Figure 2F). In the MC38 colorectal cancer model of immunocompetent C57BL/6 hosts, *Cop1* KO in cells was also able to significantly decrease tumor growth and extend mouse survival (Figures S3I–S3K). Remarkably, in MC38 cells, *Cop1* KO together with anti-PD-1 treatment *in vivo* was able to eradicate tumor growth and increase survival to 100% 60 days after tumor implantation (Figure S3K). The effect of *Cop1* KO in the MC38 colorectal cancer syngeneic model suggests that *Cop1* inhibition enhances anti-tumor immunity through a mechanism that may be applicable to other cancer types beyond TNBC.

Cop1 KO decreases macrophage infiltration by regulating macrophage-associated chemokines

Cop1 was originally discovered in *Arabidopsis* to induce targeted protein degradation (Osterlund et al., 2000). Multiple substrates of *Cop1*-mediated protein degradation in mammals with

(E) Tumor volume over time in host animals implanted with *Rosa26* KO and *Cop1* KO 4T1 mouse TNBC cells. Data are shown as mean ± SEM; n = 10 mice per group; *p < 0.05, ***p < 0.001 by one-way ANOVA with Benjamini-Hochberg post-test multiple comparison.
(F) Kaplan-Meier survival analysis of host animals bearing *Rosa26* and *Cop1* KO 4T1 tumors. The *sgCop1* cohort with anti-PD-1 treatment survived significantly longer than the other groups. n = 10 mice per group; *p < 0.05, **p < 0.01, ***p < 0.001 by log rank test.

Please cite this article in press as: Wang et al., *In vivo* CRISPR screens identify the E3 ligase *Cop1* as a modulator of macrophage infiltration and cancer immunotherapy target, Cell (2021), https://doi.org/10.1016/j.cell.2021.09.006

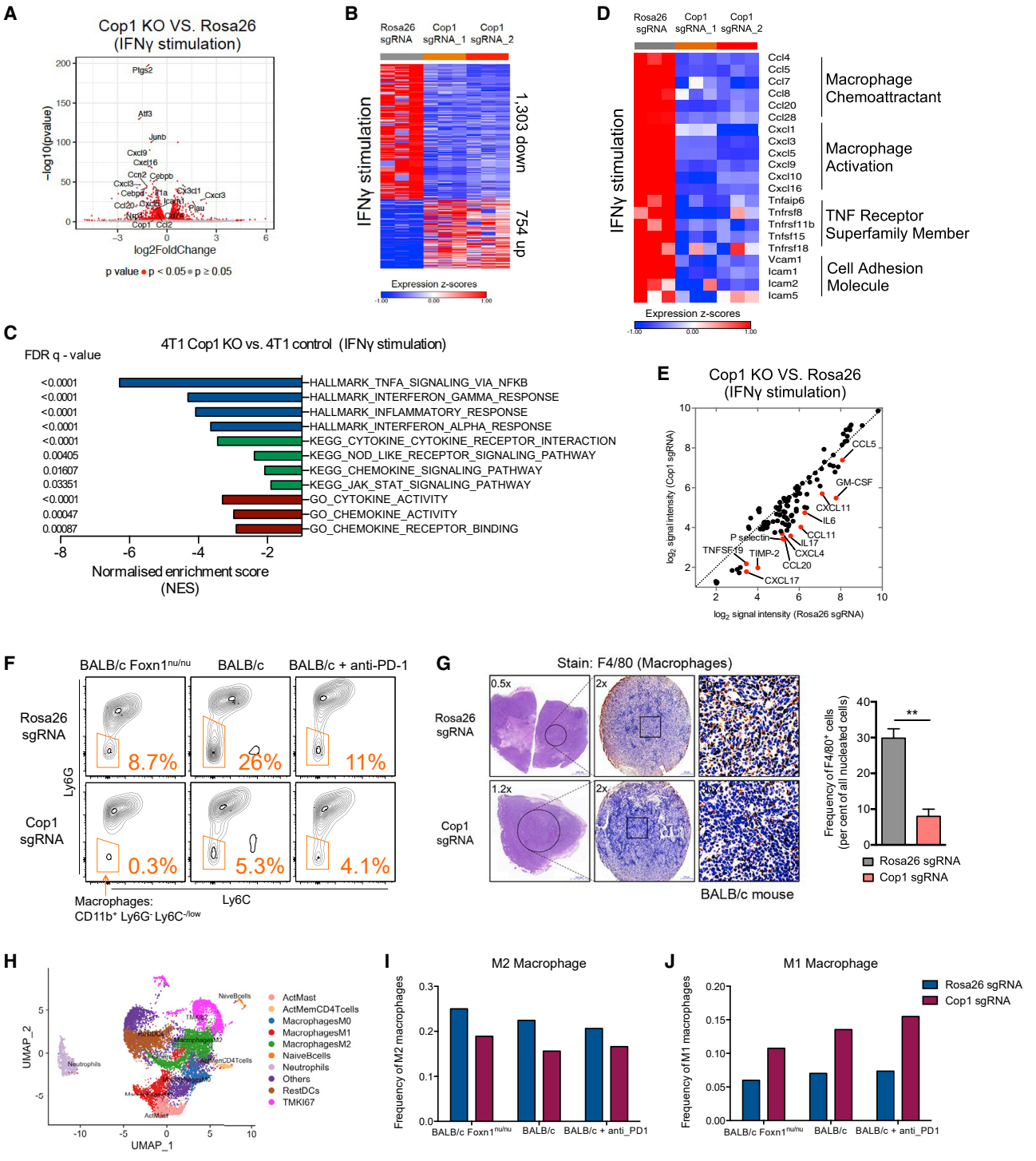

Figure 3. *Cop1* is a key mediator of macrophage chemotaxis in TNBC

(A) Volcano plot of differentially expressed genes in *Cop1* KO 4T1 mouse TNBC cells compared with *Rosa26* KO control cells with IFNγ stimulation (at 20 ng/mL for 24 h). Red dots denote genes significantly ($p < 0.05$) differentially expressed under compared conditions.

(B) Heatmap showing differential transcriptomic expression in *Rosa26* KO and *Cop1* KO 4T1 cells with IFNγ stimulation.

(C) GSEA of downregulated genes in *Cop1* KO 4T1 cancer cells compared with *Rosa26* KO control cells with IFNγ stimulation. Top depleted pathways in *Cop1* KO cells versus *Rosa26* KO control cells are shown.

(D) Differential transcriptomic expression of macrophage-related genes in *Rosa26* KO and *Cop1* KO 4T1 cells with IFNγ stimulation.

(E) Quantification of differential protein expression by cytokine array in *Rosa26* KO and *Cop1* KO 4T1 cells with IFNγ stimulation.

(legend continued on next page)

Please cite this article in press as: Wang et al., *In vivo* CRISPR screens identify the E3 ligase *Cop1* as a modulator of macrophage infiltration and cancer immunotherapy target, Cell (2021), https://doi.org/10.1016/j.cell.2021.09.006

cancer implications have been identified, including the classic tumor suppressor *Tp53* (Dornan et al., 2004a), the transcriptional regulator *c-Jun* (Savio et al., 2008; Wertz et al., 2004), and the metabolic regulator *Torc2* (Dentin et al., 2007). In humans, *COP1* is located in a region of chromosome 1 frequently amplified in individuals with breast cancer (Figure S4A) (Dornan et al., 2004b). To characterize the effects of *Cop1* on anti-tumor immunity, we first performed RNA-seq analysis of *Cop1* KO and control *Rosa26* KO in 4T1 cells under IFNγ treatment (Figure 3A). Differential expression analysis showed that 754 genes were significantly upregulated and 1,303 downregulated ($q < 0.05$) upon *Cop1* KO (Figure 3B). Gene set enrichment analysis (GSEA) showed enrichment of downregulated genes in immune-related pathways, including tumor necrosis factor alpha (TNF-α) signaling, inflammatory responses, JAK-STAT signaling pathways, and chemokine and cytokine signaling activities (Figure 3C). We also observed similar results in 4T1 cells without IFNγ stimulation (Figures S4B–S4D).

One intriguing result was that *Cop1 KO* in 4T1 cells, with or without IFNγ stimulation, resulted in significant downregulation of key macrophage chemoattractants, cytokines involved in macrophage activation, and members of the TNF receptor superfamily (Figure 3D; Figure S4E). Quantification of protein expression based on a cytokine array containing 96 cytokines confirmed significantly decreased levels of cytokines and chemokines known to recruit and activate macrophages, such as *Ccl2*, *Ccl5*, *Ccl11*, *Ccl19*, *Ccl20*, *Cxcl4*, *Cxcl11*, *Gm-csf*, and *Il-6* (Figure 3E; Figures S4F and S4G). Consistent with a decrease in cytokines and chemokines, flow cytometry and immunohistochemistry found a significant decrease in macrophage infiltration in *Cop1* KO tumors (Figures 3F and 3G; Figures S4H and S4I). In contrast, no significant change was observed in the level of tumor-infiltrating $CD8^+$ T cells, myeloid cells, and monocytes (Figures S4J–S4L). Furthermore, we confirmed the effect of *Cop1* KO in decreasing macrophage chemoattractants in tumors grown *in vivo* using the same 96-cytokine array and bulk tumor RNA-seq (Figure S4M and S4N).

To evaluate which macrophage subsets were altered, we performed single-cell transcriptomics (single-cell RNA-seq [scRNA-seq]) on triplicate tumors with *Rosa26* gRNAs and *Cop1* gRNAs. Analysis of scRNA-seq of $CD45^+$ immune cells from these KO tumors further revealed decreased M2 macrophage and increased M1 macrophage infiltration upon *Cop1* KO (Figures 3H–3J). Furthermore, in the 4T1 model, macrophage percentage in tumor-infiltrating $Cd45^+$ leukocytes was correlated positively with tumor size, whereas T cell percentage was correlated negatively (Figures S4O and S4P). Our results suggest that *Cop1* in TNBC regulates macrophage chemotaxis in the TME. Inhibition of *Cop1* decreases tumor macrophage infiltration, which, in turn, inhibits tumor progression and improves survival.

Integrated analyses identify *C/ebpδ* as a specific protein substrate of *Cop1*

We next sought to identify the putative protein substrates of the E3 ubiquitin ligase *Cop1*. Because most of the known *Cop1* substrates are transcription factors (TFs) (Dornan et al., 2004a; Janic et al., 2018; Migliorini et al., 2011; Vitari et al., 2011), we reasoned that *Cop1* KO might stabilize TFs that suppress expression of macrophage cytokines. To infer the likely TFs underlying the genes that are differentially expressed upon *Cop1* KO, we used a computational method we developed previously called LISA (Qin et al., 2020). Given a list of differentially expressed genes, LISA first estimates the epigenetic model fitting these input genes from a large compendium of publicly available histone mark and chromatin accessibility profiles in the Cistrome database and then uses TF chromatin immunoprecipitation sequencing (ChIP-seq) results and known DNA-binding motifs to infer the driving regulators (Mei et al., 2017; Zheng et al., 2019). LISA analysis of the genes downregulated upon *Cop1* KO implicated the *CEBP* and *AP-1* families of TFs as putative regulators (Figure 4A). Although a function in transcriptional repression has not yet been reported for the *CEBP* family, the *AP-1* family is known to repress gene transcription (Eferl and Wagner, 2003; Miao and Ding, 2003).

In parallel, we hypothesized that the TF substrates stabilized upon *Cop1* KO would, in turn, increase chromatin binding and the accessibility at these binding sites. We therefore performed ATAC-seq on *Cop1* KO 4T1 cells and control *Rosa26* KO 4T1 cells. Regardless of IFNγ treatment, *Cop1* KO did not change chromatin accessibility in the vast majority of the peaks (Figure 4B; Figure S5A), although there were more upregulated ATAC-seq peaks. An analysis of motif enrichment and peak overlap with public ChIP-seq data found *Cop1* KO-specific upregulated peaks to be enriched for binding by the *AP-1*, *CEBP*, and *ETS* families of TFs (Figure 4C; Figure S5B; Table S5). Therefore, the ATAC-seq data support RNA-seq analysis in implicating the *AP-1* and *CEBP* families of TFs as putative substrates of *Cop1* in 4T1 cells.

To further validate the substrates of *Cop1* protein degradation, we used mass spectrometry to identify proteins with increased abundance in *Cop1 KO* 4T1 cells compared with control cells (Figures S5C and S5D; Table S6). Among the over 7,000 detected proteins, several members of the *ETS*, *AP-1*, and *CEBP* TF families were significantly upregulated (false discovery rate [FDR] < 0.1), including the known *Cop1* substrates *c-Jun*, *Ets1*, *Ets2*, and *Etv4* (Figure 4D; Figure S5E). To rule out the possibility of non-proteasomal degradation from secondary effects, we

(F) Flow cytometry analysis of macrophage populations in *Rosa26* and *Cop1* KO 4T1 tumors grown under different host conditions *in vivo*. The tumor-infiltrating macrophages were identified as $Cd45.2^+Cd11c^{low}Cd11b^{high}Ly6C^{low}Ly6G^{low}$. The tumor-infiltrating myeloid cells were identified as $Cd45.2^+Cd11c^{low}Cd11b^{high}$.
(G) Immunohistochemistry of sections shows different macrophage infiltration in *Rosa26* and *Cop1* KO 4T1 tumors. The tumor-infiltrating macrophages were stained by immunohistochemistry with F4/80 antibody, a widely used monocyte-macrophage marker in mice. n = 5 mice per group. Data are mean ± SEM. $^{**}p < 0.01$ by two-sample t test.
(H) UMAP plot of cells from the scRNA-seq samples profiled, with each cell color coded to indicate the associated cell types.
(I) Frequency of M2 macrophages in all tumor-infiltrating CD45+ cells from control and *Cop1*-null 4T1 tumors.
(J) Frequency of M1 macrophages in all tumor-infiltrating CD45+ cells from control and *Cop1*-null 4T1 tumors.

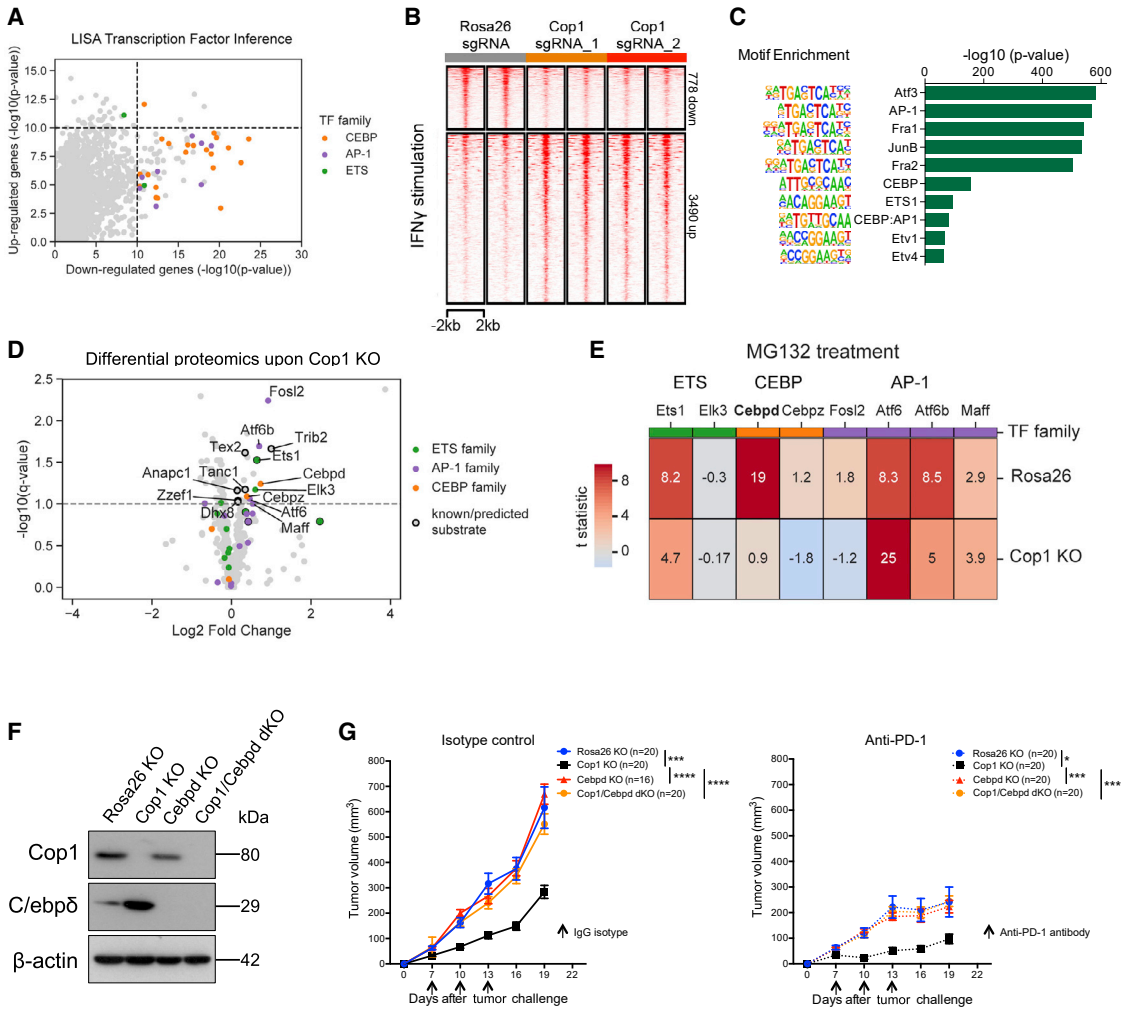

Figure 4. Integrative analysis shows that *C/ebpδ* activity is modulated upon *Cop1* KO

(A) LISA predicts CEBP and AP1 families of TFs in regulating *Cop1* KO downregulated genes.

(B) Heatmap showing changes in chromatin accessibility of *Rosa26* and *Cop1* KO 4T1 cancer cells with IFNγ stimulation (20 ng/mL for 24 h).

(C) Enrichment of known TF motifs in *Cop1* KO/*Rosa26* differential peaks.

(D) Proteomics analysis of *Rosa26* and *Cop1* KO 4T1 cancer cells. Points above the dashed line are statistically significant ($q < 0.1$).

(E) Heatmap displaying the protein abundance of genes in 4T1 cells with MG132 treatment (proteasome inhibitor). Each row shows a comparison of proteasome inhibition versus vehicle. If a protein is not degraded by the proteasomal degradation pathway, then it should show zero difference in protein expression.

(F) Western blot of *Cop1* and *C/ebpδ* protein levels in 4T1 mouse TNBC cells transduced with sgRNA targeting *Cop1*, *C/ebpδ*, and *Rosa26*.

(G) Tumor volume over time in host animals implanted with *Rosa26* KO, *Cop1* KO, *C/ebpδ* KO, and *Cop1*/*C/ebpδ* double KO 4T1 mouse TNBC cells. Data are shown as mean ± SEM; n = 10 mice per group; *$p < 0.05$, ***$p < 0.001$, ****$p < 0.001$ by one-way ANOVA with Benjamini-Hochberg multiple test correction.

conducted additional proteomics analyses after treating the cells with the proteasome inhibitor MG132. Among the proteins in the *CEBP* TF family, only *C/ebpδ* showed *Cop1*-dependent protein degradation with MG132 treatment (Figure 4E). To further evaluate the effect of *C/ebpδ* on tumor progression following *Cop1* loss of function in mouse TNBC models, we implanted 4T1 cells with only *Cop1* KO or 4T1 cells harboring *Cop1* and *C/ebpδ* KO into the mammary fat pads of BALB/c hosts (Figure 4F). We observed that tumor growth of *Cop1* KO 4T1 cells is fully rescued by *C/ebpδ* KO (Figure 4G), indicating that *C/ebpδ* accumulation induced by *Cop1* dysfunction is responsible for suppression of 4T1 tumor growth. These results provide evidence that, in 4T1 cells, *C/ebpδ* is a specific protein substrate of *Cop1* that mediates increased chromatin accessibility, decreased target gene expression, and slower tumor growth upon *Cop1* KO.

C/ebpδ suppresses expression of genes that encode macrophage-attracting chemokines in cancer cells

To map *C/ebpδ* binding sites and target genes, we performed *C/ebpδ* ChIP-seq experiments in 4T1 cells with or without *Cop1* KO. Consistent with the increased *C/ebpδ* protein abundance upon *Cop1* KO, there was an overall larger number of upregulated *C/ebpδ* binding peaks (Figure 5A) with corresponding greater chromatin accessibility (Figure 5B). Motif analysis found

Please cite this article in press as: Wang et al., *In vivo* CRISPR screens identify the E3 ligase *Cop1* as a modulator of macrophage infiltration and cancer immunotherapy target, Cell (2021), https://doi.org/10.1016/j.cell.2021.09.006

CellPress

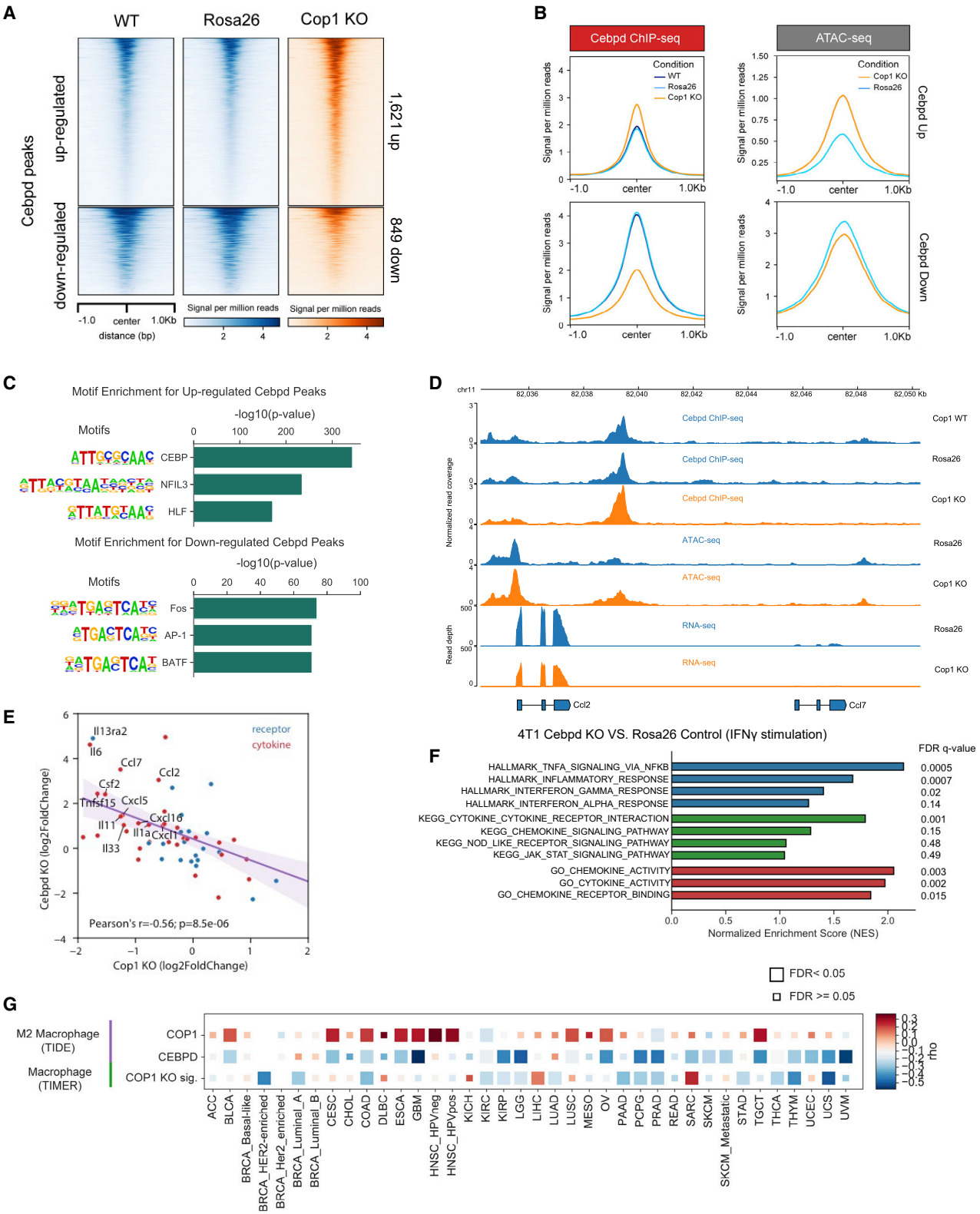

(legend on next page)

Please cite this article in press as: Wang et al., *In vivo* CRISPR screens identify the E3 ligase *Cop1* as a modulator of macrophage infiltration and cancer immunotherapy target, Cell (2021), https://doi.org/10.1016/j.cell.2021.09.006

the *CEBP* motif to be the most enriched motif in upregulated *C/ebpδ* peaks and the *AP-1* family member *Fos* motif to be most enriched in downregulated *C/ebpδ* peaks (Figure 5C). This suggests that upregulated *C/ebpδ* peaks are the primary effect of *Cop1* KO on *C/ebpδ*.

To assess which gene sets are regulated by *C/ebpδ* in 4T1 cancer cells, we evaluated the differentially expressed genes upon *Cop1* KO near the *C/ebpδ* binding sites by Cistrome-GO, an algorithm we developed previously for integrated analysis of ChIP-seq and RNA-seq data (Li et al., 2019). We found that the downregulated genes are significantly associated with regulation of immune response genes and macrophage chemokines (Figure S5F), such as *Ccl2* and *Ccl7* (Figure 5D). In contrast, *C/ebpδ* binding sites near genes that are upregulated upon *Cop1* KO are enriched in amino acid metabolism and peptide biosynthesis (Figure S5F). To further evaluate the transcriptional effects of immune response genes and macrophage chemokines by *C/ebpδ*, we performed RNA-seq analysis of *C/ebpδ* KO. We confirmed that KO of *C/ebpδ* has opposite effects compared with *Cop1* KO on regulation of cytokines and cytokine receptors, especially macrophage-related cytokines in 4T1 cells (Figure 5E; Figure S5G). Pathways downregulated upon *Cop1* KO (Figure 3C) were also upregulated in *C/ebpδ* KO (Figure 5F). Our results indicate that *Cop1* KO decreased proteasomal degradation of *C/ebpδ* and that the stabilized *C/ebpδ* suppresses transcription of immune response genes and macrophage cytokines.

To evaluate whether the *Cop1* effect on macrophage infiltration and tumor progression in mouse TNBC models (Figures 2E and 3G) is relevant in human tumors, we examined public tumor cohorts. *COP1* is more highly expressed in tumor samples compared with adjacent normal samples across many cancer types in The Cancer Genome Atlas (TCGA) (Figure S5H), including breast and colon cancers. Furthermore, *COP1* expression is positively correlated with the M2 macrophage signature inferred from previous studies (Jiang et al., 2018; Li et al., 2020), whereas *CEBPD* expression is negatively correlated with the M2 macrophage signature (Figure 5G). An *in vitro Cop1* KO signature of differentially expressed genes (STAR Methods), which may reflect *C/ebpδ* protein activity, was also correlated negatively with macrophage infiltration inferred from multiple algorithms (Li et al., 2017, 2019; Aran et al., 2017; Newman et al., 2019; Figure 5G; Figures S5I and S5J). Moreover, by analyzing the proteomics profile of different human breast and colon cancer cell lines (Nusinow et al., 2020), we confirmed the positive association between *COP1* protein and macrophage-associated cytokines in human cancer cell lines, including *CCL2*, *CCL7*, and other downregulated chemokines, upon *Cop1* KO in 4T1 cells (Figure S5K). We further evaluated the correlation between *COP1* expression and survival of affected individuals in TCGA cohorts. Lower *COP1* expression in tumors is associated with better outcomes in multiple cancer types, including breast cancer, ovarian cancer, and papillary kidney cancers (Figures S5L–S5N). These data indicate a robust association of high *Cop1* and low *C/ebpδ* expression with increased macrophage infiltration across human cancers.

Cop1 targets *C/ebpδ* for proteasome degradation via the scaffolding protein *Trib2*

To elucidate how *Cop1* degrades the *C/ebpδ* protein, we screened proteins that were upregulated upon *Cop1* KO for the presence of a predicted *Cop1* degron motif (Figures S6A–S6C). To this end, we applied a machine learning approach (see STAR Methods for further details) that was predictive of previously reported degrons in known *Cop1* substrates (Figure S6B). This analysis predicted several proteins as the most likely direct *Cop1* substrates in 4T1, including *Trib2 (*Tribbles homolog 2), *Tanc1* (tetratricopeptide repeat, ankyrin repeat and coiled-coil containing 1), *Tex2* (testis expressed 2), and the known substrate *Ets1* (ETS proto-oncogene 1) (Figure 4D; see STAR Methods for further details). Surprisingly, the predicted substrates did not include *C/ebpδ* or any *CEBP* family member, suggesting that *C/ebpδ* might be an indirect substrate of *Cop1*. We noted that *Trib2*, the protein with a *Cop1* degron whose level is most elevated upon *Cop1* KO, has been reported previously to serve as a substrate adaptor for *Cop1* to modulate its specificity (Figure S6D; Keeshan et al., 2006). *TRIB* family pseudokinases possess a C-terminal tail that serves as a peptide motif for MAPKK/MEK family members and a second binding motif that facilitates direct association with E3 ubiquitin ligases (Eyers et al., 2017). In human or mouse acute myeloid leukemia (AML), TRIB pseudokinases are known to provide a unique molecular scaffold bound by *C/ebpα* and *Cop1* (Eyers et al., 2017; Jamieson et al., 2018; Murphy et al., 2015). Notably, C/*ebpδ*, but not C/*ebpα*, was detected at the protein level in 4T1 cells. Based on this, we hypothesized that *Trib2* might serve as an adaptor to facilitate the interaction between *C/ebpδ* and *Cop1*, leading to *Cop1*-mediated proteasomal degradation of *C/ebpδ* (Figure 6A).

To test this hypothesis, we first performed co-immunoprecipitation (coIP) in wild-type 4T1 cells. This confirmed co-binding of endogenous *Cop1*, *Trib2*, and *C/ebpδ* (Figure 6B; Figures S6E and S6F). Furthermore, we found that, although *Cop1* KO did not significantly increase *Trib2* and *C/ebpδ* mRNA levels (Figure S6G), it significantly increased their protein levels (Figure 6C).

Figure 5. The *COP1* axis is associated with macrophage infiltration and response to ICB for individuals with cancer

(A) Distribution of normalized read counts in a 2,000-bp window around *Cop1* KO-specific *C/ebpδ* peaks.

(B) Distribution of gene-averaged read counts for the datasets of *C/ebpδ* ChIP-seq and ATAC-seq.

(C) Significant *de novo* motifs of *Cop1* KO-specific *C/ebpδ* peaks. The p values were determined by hypergeometric test.

(D) Normalized signal tracks of ChIP-seq, ATAC-seq, and RNA-seq at the Ccl2 and Ccl7 loci in 4T1 cancer cells.

(E) Correlation of differential expression (log fold change) of cytokines and cytokine receptors between *Cop1* KO and *C/ebpδ* KO.

(F) GSEA of upregulated genes in *C/ebpδ* KO 4T1 cancer cells compared with *Rosa26* KO control cells with IFNγ stimulation.

(G) Heatmap showing the correlation between gene expression of *COP1* or *CEBPD* with inferred macrophage infiltration in The Cancer Genome Atlas (TCGA). *CEBPD* expression was correlated negatively with M2 macrophages (TIDE). Correlations were obtained through the TIMER website and adjusted for tumor purity. Cancer types are labeled on the x axis.

Please cite this article in press as: Wang et al., *In vivo* CRISPR screens identify the E3 ligase *Cop1* as a modulator of macrophage infiltration and cancer immunotherapy target, Cell (2021), https://doi.org/10.1016/j.cell.2021.09.006

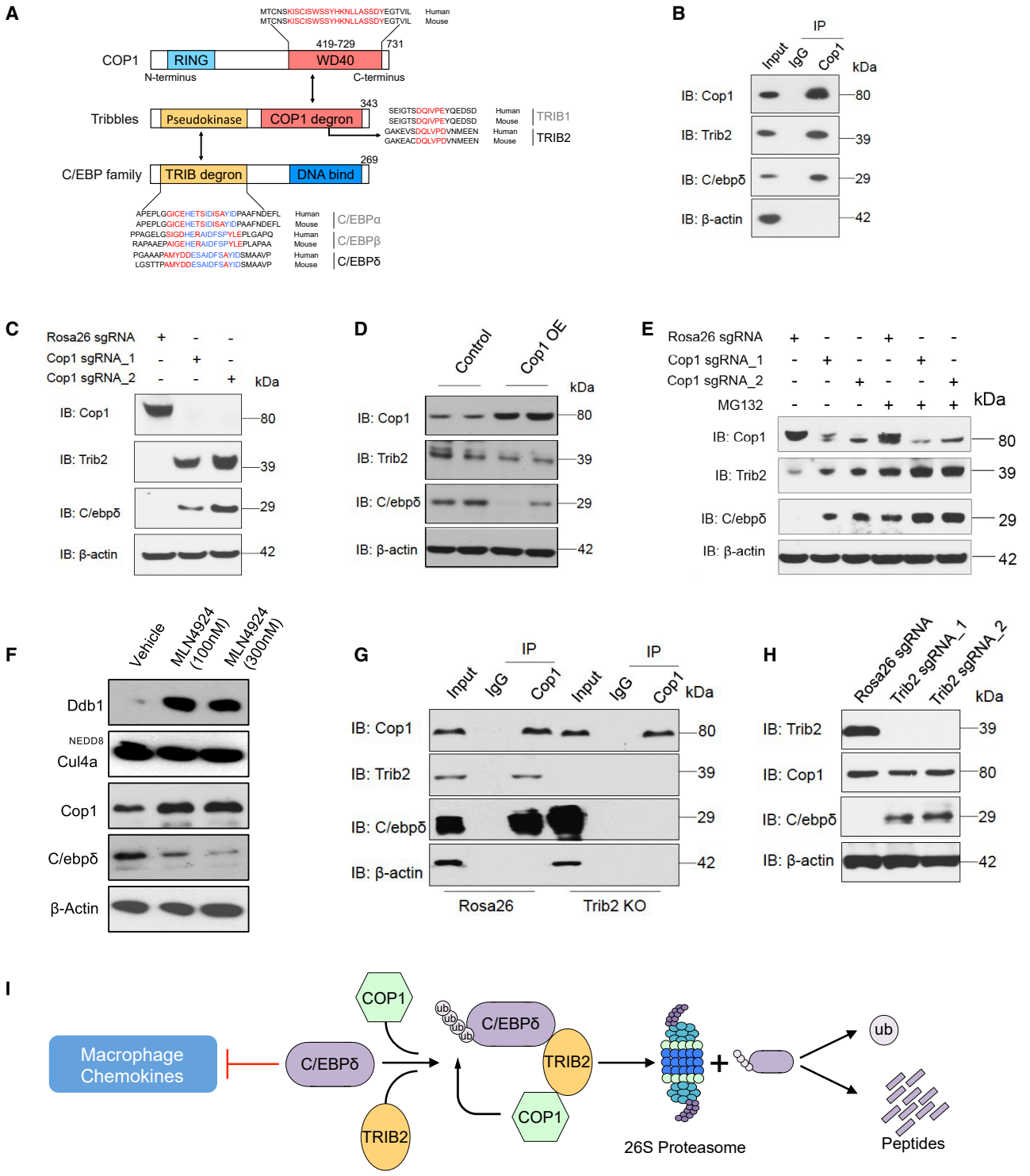

Figure 6. Identification of *C/ebpδ* as a direct target of *Cop1* via the adaptor *Trib2*

(A) Schematic illustrating motifs of CEBP family members bound by Tribbles-*Cop1*.

(B) The lysate from wild-type 4T1 cells was incubated with *Cop1* antibody or control immunoglobulin G (IgG), and the immunocomplexes were probed with the indicated antibodies.

(C) Western blot showing representative protein levels of *Cop1*, *Trib2*, and *C/ebpδ* in *Rosa26* KO and *Cop1* KO cancer cells.

(D) Western blot showing representative protein levels of *Cop1*, *Trib2*, and *C/ebpδ* in *Cop1*-overexpressing and control 4T1 cells.

(E) Western blot showing representative protein levels of *Cop1*, *Trib2*, and *C/ebpδ* in *Cop1* KO and *Rosa26* KO 4T1 cancer cells with or without MG132 treatment.

(legend continued on next page)

Please cite this article in press as: Wang et al., *In vivo* CRISPR screens identify the E3 ligase *Cop1* as a modulator of macrophage infiltration and cancer immunotherapy target, Cell (2021), https://doi.org/10.1016/j.cell.2021.09.006

In addition, forced overexpression of *Cop1* led to a decreased *C/ebpδ* protein level without affecting its mRNA (Figure 6D; Figure S6H), supporting *C/ebpδ* post-translational regulation by *Cop1*.

To confirm that *C/ebpδ* degradation is mediated by the proteasome pathway, we treated 4T1 cells with the selective proteasome inhibitor MG132. We observed that, with proteasome inhibition, the *Trib2* and *C/ebpδ* proteins were significantly more abundant than in wild-type cells regardless of *Cop1* status (Figure 6E). Moreover, the polyubiquitination level of *C/ebpδ* was attenuated by *Cop1* KO in 4T1 cells and elevated with proteasome inhibition (Figure S6I). These results indicate that *Cop1* can induce degradation of *C/ebpδ* through a proteasomal degradation pathway.

Cop1-dependent proteasomal degradation is notoriously complex (Marine, 2012). It has been reported that *Cop1* can directly induce transfer of ubiquitin from E2 proteins to some of its substrates (Dornan et al., 2004a; Seo et al., 2003) or indirectly promote degradation by linking some substrates to an E3 ligase complex, such as the *CUL4A-DDB1* complex (Vitari et al., 2011; Wertz et al., 2004). We evaluated whether *Cop1* acts as an adaptor protein by bringing *C/ebpδ* to the *Cul4a-Ddb1* E3 ubiquitin ligase complex for degradation. We treated 4T1 cells with the neddylation inhibitor MLN4924 and observed decreased *C/ebpδ* protein levels under neddylation inhibitor treatment (Figure 6F), suggesting that *C/ebpδ* degradation by *Cop1* works through a Cullin-independent mechanism.

Finally, to prove that *Trib2* is important in mediating *Cop1* degradation of *C/ebpδ*, we used CRISPR to knock out *Trib2*. This not only disrupted the interaction between *Cop1* and *C/ebpδ* (Figure 6G) but also increased the level of *C/ebpδ* protein (Figure 6H). These results indicate that, in 4T1 cancer cells, *C/ebpδ* is a substrate of *Cop1* and that the interaction between *Cop1* and *C/ebpδ* is mediated by *Trib2*, which results in ubiquitination and proteasomal degradation of *C/ebpδ* (Figure 6I). *Cop1* inhibition, which stabilizes *C/ebpδ* to suppress macrophage chemoattractant release, can increase tumor sensitivity to immunity and immunotherapy (Figure S6J).

DISCUSSION

TNBC has an immunosuppressive TME, preventing an effective response to ICB therapies. There is an urgent need to identify new targets to reprogram the suppressive TNBC TME to enhance immunotherapy efficacy. In this study, we used large-scale CRISPR KO screens to discover genes that sensitize TNBC to anti-tumor immunity in host mice that differ in microenvironmental competency. We found that the E3 ubiquitin ligase *Cop1* regulates the protein abundance of the TF *C/ebpδ* via the adaptor protein *Trib2*. *C/ebpδ* transcriptionally suppresses macrophage chemoattractant release from cancer cells. *Cop1* inhibition in TNBCs leads to decreased macrophage infiltration, increased sensitivity to anti-PD-1 treatment, and better survival in mouse models. We also observed associations between *COP1* expression, levels of macrophage infiltration, and clinical outcomes in many human cancer types. Our study establishes a role of *Cop1* in modulating macrophage infiltration into tumors and in suppressing the effects of immunotherapies.

Activation of the IFNγ signaling pathway in cancer cells has long been considered to facilitate T cell antigen recognition and activate T cell cytotoxicity (Gao et al., 2016). Paradoxically, we found breast cancer cells to be sensitized to immunotherapy by loss of function of *Jak1*, *Stat1*, or *Irf1*, downstream effectors of the IFNγ signaling pathway. Supporting our observation, loss of *Jak1* has been reported to prevent progression of breast cancer in mammary cancer models (Chen et al., 2018b; Wehde et al., 2018). Studies in breast cancer and melanoma models also found that sustained IFNγ activation could have the opposite effect as short-term IFNγ treatment, inducing resistance to immunotherapy (Benci et al., 2016; Jacquelot et al., 2019). This may explain why early-phase clinical trials of IFNγ failed in individuals with melanoma (Meyskens et al., 1990, 1995). Therefore, the anti- and pro-tumor functions of IFNγ might depend on the tumor context, microenvironmental factors, signaling intensity, and signaling duration.

Over the past decade, *Cop1* has been found to play an important role in tumor growth and metastasis (Wei and Kaelin, 2011). A number of potential *Cop1* degradation substrates have been identified, including *Tp53*, *c-Jun*, *Cebpa*, *Mek1*, *p65/RelA*, *Mkk4*, *Acc1*, *Mta1*, *Foxo1*, *Torc2*, and *Pea3* (Dornan et al., 2004a; Janic et al., 2018; Migliorini et al., 2011; Wei and Kaelin, 2011). With oncogene and tumor suppressor proteins as putative *Cop1* substrates, characterization of *Cop1* as an oncogene or a tumor suppressor has been inconsistent. Analysis of *COP1* essentiality based on CRISPR screens of hundreds of cancer cell lines in the Dependency Map project shows generally weak effects on cell growth in human cancer cell lines *in vitro* (Tsherniak et al., 2017). This is consistent with the *Cop1* KO phenotype we observed in mouse breast cancer (4T1) and colorectal cancer (MC38) cells grown *in vitro*. At the same time, *Cop1* KO significantly suppressed tumor growth and prolonged survival in wild-type mice, especially mice treated with ICB, compared with nude mice. This suggests that the effects of *Cop1* on tumor progression act through TME reprogramming and immune response, implicating *Cop1* as an immunotherapy target. In addition, our study revealed a possible mechanism of tumor growth suppression through decreased macrophage recruitment. However, cytokines and chemokines regulated by the *Cop1-C/ebpδ* pathway may influence not only macrophages but also other immune cell types in the TME. For example, Ccl2 was discovered as a chemoattractant for macrophages, but it also attracts monocytes, MDSCs, lymphocytes, and neutrophils under specific conditions (Gschwandtner et al., 2019). Therefore, it will be important to explore the effects of

(F) Protein levels of *Ddb1*, *Cul4a*, *Cop1* and *C/ebpδ* in 4T1 cancer cells under treatment of neddylation inhibitor MLN4924.
(G) CoIP experiment with *Cop1* antibody for *Rosa26* KO and *Trib2* KO 4T1 cells.
(H) Western blot comparing *Trib2* KO and *Rosa26* KO (control) 4T1 cancer cells for protein levels of Cop1, Trib2, and Cebpd.
(I) Schematic illustrating degradation of *C/ebpδ* by *Trib2-Cop1*.

Please cite this article in press as: Wang et al., *In vivo* CRISPR screens identify the E3 ligase *Cop1* as a modulator of macrophage infiltration and cancer immunotherapy target, Cell (2021), https://doi.org/10.1016/j.cell.2021.09.006

cytokines regulated by *Cop1-C/ebpδ* on other immune cell types. At the same time, we note that *Cop1* is not only expressed in cancer cells but also in immune cells and in normal tissues. Therefore, future studies must evaluate systemic effects of *Cop1* inhibition *in vivo* or in human cancers, especially when a small-molecule inhibitor of *Cop1* is employed.

Our study found that, in cancer cells, *Cop1* affects cancer progression through its influence on *C/ebpδ* proteasomal degradation. The *CEBP* family of TFs is known to regulate many biological processes, including cell differentiation, motility, proliferation, cell death, metabolism, and immune responses (Ko et al., 2015). A previous study reported that *C/ebpα* stability is required to prevent *Trib1-Cop1* complex-driven AML (Nakamae et al., 2017). Another study found that aberrant *C/ebpα* protein levels caused by *Trib1* deficiency in hematopoietic cells results in severe reduction of M2-like macrophages in the bone marrow, spleen, lungs, and adipose tissue (Satoh et al., 2013). A more recent study of Alzheimer's disease reported that *C/EBPβ* in microglia, which drives a potent proinflammatory program, is regulated at the protein level by *COP1* (Ndoja et al., 2020). In this study, we further showed the effect of *Cop1* on macrophage infiltration and tumor growth through *Trib2* and *C/ebpδ* in solid tumors. In addition, *COP1* expression is associated with high macrophage infiltration, and the *Cop1* KO signature is associated with low macrophage infiltration across many human cancer types.

Although the level of *C/ebpδ* protein is the most significantly changed CEBP family member upon *Cop1* KO, it is not the only *CEBP* family member whose protein levels are affected. It is possible that, in other cancer types or immune cells, *Cop1* KO could stabilize other *CEBP* family members that function in suppressing macrophage infiltration and tumor growth. In addition, our RNA-seq, ATAC-seq, and proteomics analyses suggest that the *AP-1* family of TFs might interact with *C/ebpδ* or mediate secondary effects upon *Cop1* KO. Further studies are needed to pinpoint the specific *AP-1* family members involved and to elucidate this interaction and its effect.

Currently available ICB antibodies, such as anti-PD-1, anti-PD-L1, and anti-CTLA4, aim to facilitate cancer cell recognition by lymphocytes and increase T cell cytotoxicity. However, the majority of human tumors, especially from breast, prostate, colon, and lung cancers, are tumors with low levels of cytotoxic T lymphocytes (CTLs), and most tumors generally elicit low immune activity. Therefore, recent cancer immunology research and immune-oncology drug development have been focused on reprogramming the TME by killing immunosuppressive fibroblasts (Noy and Pollard, 2014) or macrophages (Motz and Coukos, 2013) to help T cell infiltration. The fact that different syngeneic tumor models have such different TMEs indicates that cancer-cell-intrinsic mechanisms may determine whether a tumor supports an effective or ineffective immune response. Our study, together with previous work (Codina et al., 2019; Lawson et al., 2020; Li et al., 2020; Manguso et al., 2017), demonstrates the effectiveness of *in vivo* CRISPR screens in identifying such cancer-cell-intrinsic TME regulators. However, in the TME, it is possible that the cytokine effects derived from cancer cells on immune cells are short ranged; then, heterogeneous distributions of cytokines are a potential reason influencing the cell-extrinsic effects. These *in vivo* studies could only test a restricted set of genes in a limited number of syngeneic tumor models. Similar approaches applied to more genes in additional syngeneic models are likely to identify additional targets that can reprogram the TME to enhance immunotherapy response.

LIMITATIONS OF THE STUDY

Our observation showed that loss of the E3 ubiquitin ligase *Cop1* in TNBC cancer cells decreases secretion of macrophage-associated chemokines, reduces tumor macrophage infiltration, enhances antitumor immunity, and strengthens ICB response. We found that the effects of Cop1 on gene expression are largely mediated by proteasomal degradation of the *C/ebpδ* protein, but the mechanisms of *C/ebpδ*'s regulation of downstream gene expression need better characterization. Our preliminary data showed that genes with the highest *C/ebpδ* binding can be upregulated or downregulated in *C/ebpδ*-KO cells, suggesting context-dependent gene expression regulation. Further studies are needed to elucidate the regulatory mechanisms. Furthermore, *Cop1* has not been targeted successfully with effective therapeutic drugs, limiting the immediate translational value of targeting *Cop1*. However, recent studies have developed small-molecule and/or PROTAC inhibitors for multiple other E3 ubiquitin ligases, such as *MDM2* (Tisato et al., 2017; Wachter et al., 2017), *cIAP* (Sun et al., 2014), *TRIM24* (Gechijian et al., 2018), and *DCAF16* (Zhang et al., 2019). We expect that *Cop1*-targeting inhibitors can be developed in the near future to potentiate ICB therapy in TNBC.

STAR★METHODS

Detailed methods are provided in the online version of this paper and include the following:

- KEY RESOURCES TABLE
- RESOURCE AVAILABILITY
  - Lead contact
  - Materials availability
  - Data and code availability
- EXPERIMENTAL MODEL AND SUBJECT DETAILS
  - Mice
  - Cell Lines
- METHOD DETAILS
  - Large-scale mouse CRISPR library cloning
  - Viral library production
  - Viral transduction of cancer cells
  - Genomic DNA extraction
  - sgRNA library readout by deep sequencing
  - Generation of artificial antigen expression lentiviral vectors
  - Generation of artificial tumor antigen Ova-expressing cell lines
  - *In vivo* CRISPR screening in murine cancer cells
  - Mouse validation assays
  - Cell viability assays

- Western blot of protein expression in murine cancer cells
- Tissue processing and flow cytometry
- *In vivo* competition assays
- *In vitro* and *in vivo* chemokine measurement
- Generation of CRISPR/Cas9 Knockout cells
- RNA-seq
- Real-time reverse transcription-PCR
- ATAC-seq
- ChIP-seq
- Co-immunoprecipitation
- Single-cell RNA-seq of tumor infiltrating immune cells

● QUANTIFICATION AND STATISTICAL ANALYSIS

- Software used in this study
- CRISPR screen data analysis
- Data analysis of RNA-seq
- ATAC-seq analysis
- Single cell RNA-seq data analysis
- Data analysis of ChIP-seq
- Cop1 degron motif prioritization
- Machine learning prioritization
- Cop1 Degron Motif Filtering
- Gene signature analysis
- TCGA expression data
- Correlation with Immune Cell Infiltration
- Cytokine and surface receptor/ligand genes

SUPPLEMENTAL INFORMATION

Supplemental information can be found online at https://doi.org/10.1016/j.cell.2021.09.006.

ACKNOWLEDGMENTS

The authors would like to thank Jin Zhao and Jingyu Peng for assistance and discussions. This study was supported by the Breast Cancer Research Foundation (BCRF-20-100 to X.S.L. and BCRF-20-019 to M.B.), NIH grants R01CA234018 (to X.S.L. and M.B.), Damon Runyon Cancer Research Foundation DRQ-04-20 (to C.T.), the Sara Elizabeth O'Brien Trust (to S.S.G.), and the Dana-Farber Cancer Institute.

AUTHOR CONTRIBUTIONS

X.S.L., M.B., and X.W. conceived, designed, and initiated the study. X.W., S.S.G., N.T., Q.T., and T.X. generated lentiCRISPR vectors and libraries (MusCK 1.0 and 2.0). X.W., Q.T., S.S.G., and N.T. performed most *in vivo* experiments. X.W. and N.T. performed cell competition assays. C.T., B.W., W.L., and P.J. analyzed CRISPR screen data. B.W. analyzed RNA-seq and ATAC-seq data. C.T. analyzed ChIP-seq and proteomics data. X.W. and Y.L. performed biochemistry experiments. Q.T., B.Z., Z.L., and K.L. assisted X.W. with various experiments. N.T. assisted X.W. with histology experiments. P.C., B.Z., P.J., and H.L. provided suggestions for the ATAC-seq experiment and data analysis. Q.T., B.Z., C.M., Y.Z., Z.Z., and J.F. provided suggestions for ChIP-seq and single-cell RNA-seq data analyses. X.S.L., M.B., X.W., C.T., Q.T., and S.S.G. jointly prepared the manuscript with input from all authors. X.S.L. and M.B. secured funding and supervised the work.

DECLARATION OF INTERESTS

X.S.L. is a cofounder, board member, scientific advisor board member, and consultant of GV20 Oncotherapy and a stockholder of BMY, TMO, WBA, ABT, ABBV, and JNJ and receives research funding from Takeda, Sanofi, Bristol Myers Squibb, and Novartis. M.B. receives sponsored research support from and is a consultant to Novartis. M.B. serves on the scientific advisory boards of GV20 Oncotherapy, Kronos Bio, and H3 Biomedicine. T.X. is a cofounder, board member, and full-time employee of GV20 Oncotherapy.

Received: November 25, 2020
Revised: June 14, 2021
Accepted: September 1, 2021
Published: September 27, 2021

REFERENCES

Alshaker, H.A., and Matalka, K.Z. (2011). IFN-γ, IL-17 and TGF-β involvement in shaping the tumor microenvironment: The significance of modulating such cytokines in treating malignant solid tumors. Cancer Cell Int. *11*, 33.

Aran, D., Hu, Z., and Butte, A.J. (2017). xCell: digitally portraying the tissue cellular heterogeneity landscape. Genome Biol. *18*, 220.

Beatty, G.L., and Paterson, Y. (2000). IFN-gamma can promote tumor evasion of the immune system in vivo by down-regulating cellular levels of an endogenous tumor antigen. J. Immunol. *165*, 5502–5508.

Becht, E., Giraldo, N.A., Lacroix, L., Buttard, B., Elarouci, N., Petitprez, F., Selves, J., Laurent-Puig, P., Sautès-Fridman, C., Fridman, W.H., and de Reyniès, A. (2016). Estimating the population abundance of tissue-infiltrating immune and stromal cell populations using gene expression. Genome Biol. *17*, 218.

Benci, J.L., Xu, B., Qiu, Y., Wu, T.J., Dada, H., Twyman-Saint Victor, C., Cucolo, L., Lee, D.S.M., Pauken, K.E., Huang, A.C., et al. (2016). Tumor Interferon Signaling Regulates a Multigenic Resistance Program to Immune Checkpoint Blockade. Cell *167*, 1540–1554.e12.

Benci, J.L., Johnson, L.R., Choa, R., Xu, Y., Qiu, J., Zhou, Z., Xu, B., Ye, D., Nathanson, K.L., June, C.H., et al. (2019). Opposing Functions of Interferon Coordinate Adaptive and Innate Immune Responses to Cancer Immune Checkpoint Blockade. Cell *178*, 933–948.e14.

Bianchini, G., Balko, J.M., Mayer, I.A., Sanders, M.E., and Gianni, L. (2016). Triple-negative breast cancer: challenges and opportunities of a heterogeneous disease. Nat. Rev. Clin. Oncol. *13*, 674–690.

Burr, M.L., Sparbier, C.E., Chan, Y.-C., Williamson, J.C., Woods, K., Beavis, P.A., Lam, E.Y.N., Henderson, M.A., Bell, C.C., Stolzenburg, S., et al. (2017). CMTM6 maintains the expression of PD-L1 and regulates anti-tumour immunity. Nature *549*, 101–105.

Cassetta, L., and Pollard, J.W. (2018). Targeting macrophages: therapeutic approaches in cancer. Nat. Rev. Drug Discov. *17*, 887–904.

Cassetta, L., Fragkogianni, S., Sims, A.H., Swierczak, A., Forrester, L.M., Zhang, H., Soong, D.Y.H., Cotechini, T., Anur, P., Lin, E.Y., et al. (2019). Human Tumor-Associated Macrophage and Monocyte Transcriptional Landscapes Reveal Cancer-Specific Reprogramming, Biomarkers, and Therapeutic Targets. Cancer Cell *35*, 588–602.e10.

Chen, C.-H., Xiao, T., Xu, H., Jiang, P., Meyer, C.A., Li, W., Brown, M., and Liu, X.S. (2018a). Improved design and analysis of CRISPR knockout screens. Bioinformatics *34*, 4095–4101.

Chen, M., Pockaj, B., Andreozzi, M., Barrett, M.T., Krishna, S., Eaton, S., Niu, R., and Anderson, K.S. (2018b). JAK2 and PD-L1 Amplification Enhance the Dynamic Expression of PD-L1 in Triple-negative Breast Cancer. Clin. Breast Cancer *18*, e1205–e1215.

Codina, A., Renauer, P.A., Wang, G., Chow, R.D., Park, J.J., Ye, H., Zhang, K., Dong, M.B., Gassaway, B., Ye, L., et al. (2019). Convergent Identification and Interrogation of Tumor-Intrinsic Factors that Modulate Cancer Immunity In Vivo. Cell Syst. *8*, 136–151.e7.

Coussens, L.M., Zitvogel, L., and Palucka, A.K. (2013). Neutralizing tumor-promoting chronic inflammation: a magic bullet? Science *339*, 286–291.

de Sena Brandine, G., and Smith, A.D. (2019). Falco: high-speed FastQC emulation for quality control of sequencing data. F1000Res. *8*, 1874.

Please cite this article in press as: Wang et al., *In vivo* CRISPR screens identify the E3 ligase *Cop1* as a modulator of macrophage infiltration and cancer immunotherapy target, Cell (2021), https://doi.org/10.1016/j.cell.2021.09.006

Dentin, R., Liu, Y., Koo, S.-H., Hedrick, S., Vargas, T., Heredia, J., Yates, J., 3rd, and Montminy, M. (2007). Insulin modulates gluconeogenesis by inhibition of the coactivator TORC2. Nature *449*, 366–369.

Dersh, D., Phelan, J.D., Gumina, M.E., Wang, B., Arbuckle, J.H., Holly, J., Kishton, R.J., Markowitz, T.E., Seedhom, M.O., Fridlyand, N., et al. (2021). Genome-wide Screens Identify Lineage- and Tumor-Specific Genes Modulating MHC-I- and MHC-II-Restricted Immunosurveillance of Human Lymphomas. Immunity *54*, 116–131.e10.

Dobin, A., Davis, C.A., Schlesinger, F., Drenkow, J., Zaleski, C., Jha, S., Batut, P., Chaisson, M., and Gingeras, T.R. (2013). STAR: ultrafast universal RNA-seq aligner. Bioinformatics *29*, 15–21.

Doench, J.G., Fusi, N., Sullender, M., Hegde, M., Vaimberg, E.W., Donovan, K.F., Smith, I., Tothova, Z., Wilen, C., Orchard, R., et al. (2016). Optimized sgRNA design to maximize activity and minimize off-target effects of CRISPR-Cas9. Nat. Biotechnol. *34*, 184–191.

Dong, H., Zhu, G., Tamada, K., and Chen, L. (1999). B7-H1, a third member of the B7 family, co-stimulates T-cell proliferation and interleukin-10 secretion. Nat. Med. *5*, 1365–1369.

Dornan, D., Wertz, I., Shimizu, H., Arnott, D., Frantz, G.D., Dowd, P., O'Rourke, K., Koeppen, H., and Dixit, V.M. (2004a). The ubiquitin ligase COP1 is a critical negative regulator of p53. Nature *429*, 86–92.

Dornan, D., Bheddah, S., Newton, K., Ince, W., Frantz, G.D., Dowd, P., Koeppen, H., Dixit, V.M., and French, D.M. (2004b). COP1, the negative regulator of p53, is overexpressed in breast and ovarian adenocarcinomas. Cancer Res. *64*, 7226–7230.

Eeckhoute, J., Keeton, E.K., Lupien, M., Krum, S.A., Carroll, J.S., and Brown, M. (2007). Positive cross-regulatory loop ties GATA-3 to estrogen receptor alpha expression in breast cancer. Cancer research *67* (13), 6477–6483.

Eferl, R., and Wagner, E.F. (2003). AP-1: a double-edged sword in tumorigenesis. Nat. Rev. Cancer *3*, 859–868.

Eyers, P.A., Keeshan, K., and Kannan, N. (2017). Tribbles in the 21st Century: The Evolving Roles of Tribbles Pseudokinases in Biology and Disease. Trends Cell Biol. *27*, 284–298.

Fallahpour, S., Navaneelan, T., De, P., and Borgo, A. (2017). Breast cancer survival by molecular subtype: a population-based analysis of cancer registry data. CMAJ Open *5*, E734–E739.

Fei, T., Chen, Y., Xiao, T., Li, W., Cato, L., Zhang, P., Cotter, M.B., Bowden, M., Lis, R.T., Zhao, S.G., et al. (2017). Genome-wide CRISPR screen identifies HNRNPL as a prostate cancer dependency regulating RNA splicing. Proc. Natl. Acad. Sci. USA *114*, E5207–E5215.

Finotello, F., Mayer, C., Plattner, C., Laschober, G., Rieder, D., Hackl, H., Krogsdam, A., Loncova, Z., Posch, W., Wilflingseder, D., et al. (2019). Molecular and pharmacological modulators of the tumor immune contexture revealed by deconvolution of RNA-seq data. Genome Med. *11*, 34.

Freeman, G.J., Long, A.J., Iwai, Y., Bourque, K., Chernova, T., Nishimura, H., Fitz, L.J., Malenkovich, N., Okazaki, T., Byrne, M.C., et al. (2000). Engagement of the PD-1 immunoinhibitory receptor by a novel B7 family member leads to negative regulation of lymphocyte activation. J. Exp. Med. *192*, 1027–1034.

Gao, J., Shi, L.Z., Zhao, H., Chen, J., Xiong, L., He, Q., Chen, T., Roszik, J., Bernatchez, C., Woodman, S.E., et al. (2016). Loss of IFN-γ Pathway Genes in Tumor Cells as a Mechanism of Resistance to Anti-CTLA-4 Therapy. Cell *167*, 397–404.e9.

Gechijian, L.N., Buckley, D.L., Lawlor, M.A., Reyes, J.M., Paulk, J., Ott, C.J., Winter, G.E., Erb, M.A., Scott, T.G., Xu, M., et al. (2018). Functional TRIM24 degrader via conjugation of ineffectual bromodomain and VHL ligands. Nat. Chem. Biol. *14*, 405–412.

Ginhoux, F., and Jung, S. (2014). Monocytes and macrophages: developmental pathways and tissue homeostasis. Nat. Rev. Immunol. *14*, 392–404.

Gouw, M., Michael, S., Sámano-Sánchez, H., Kumar, M., Zeke, A., Lang, B., Bely, B., Chemes, L.B., Davey, N.E., Deng, Z., et al. (2018). The eukaryotic linear motif resource - 2018 update. Nucleic Acids Res. *46* (D1), D428–D434.

Grivennikov, S.I., Greten, F.R., and Karin, M. (2010). Immunity, inflammation, and cancer. Cell *140*, 883–899.

Groner, A.C., Cato, L., de Tribolet-Hardy, J., Bernasocchi, T., Janouskova, H., Melchers, D., Houtman, R., Cato, A.C.B., Tschopp, P., Gu, L., et al. (2016). TRIM24 Is an Oncogenic Transcriptional Activator in Prostate Cancer. Cancer Cell *29*, 846–858.

Gschwandtner, M., Derler, R., and Midwood, K.S. (2019). More Than Just Attractive: How CCL2 Influences Myeloid Cell Behavior Beyond Chemotaxis. Front. Immunol. *10*, 2759.

Gu, S.S., Zhang, W., Wang, X., Jiang, P., Traugh, N., Li, Z., Meyer, C., Stewig, B., Xie, Y., Bu, X., et al. (2021). Therapeutically Increasing MHC-I Expression Potentiates Immune Checkpoint Blockade. Cancer Discov. *11*, 1524–1541.

Halle, S., Halle, O., and Förster, R. (2017). Mechanisms and Dynamics of T Cell-Mediated Cytotoxicity In Vivo. Trends Immunol. *38*, 432–443.

Hanahan, D., and Weinberg, R.A. (2011). Hallmarks of cancer: the next generation. Cell *144*, 646–674.

Ishizuka, J.J., Manguso, R.T., Cheruiyot, C.K., Bi, K., Panda, A., Iracheta-Vellve, A., Miller, B.C., Du, P.P., Yates, K.B., Dubrot, J., et al. (2019). Loss of ADAR1 in tumours overcomes resistance to immune checkpoint blockade. Nature *565*, 43–48.

Jacquelot, N., Yamazaki, T., Roberti, M.P., Duong, C.P.M., Andrews, M.C., Verlingue, L., Ferrere, G., Becharef, S., Vétizou, M., Daillère, R., et al. (2019). Sustained Type I interferon signaling as a mechanism of resistance to PD-1 blockade. Cell Res. *29*, 846–861.

Jamieson, S.A., Ruan, Z., Burgess, A.E., Curry, J.R., McMillan, H.D., Brewster, J.L., Dunbier, A.K., Axtman, A.D., Kannan, N., and Mace, P.D. (2018). Substrate binding allosterically relieves autoinhibition of the pseudokinase TRIB1. Sci. Signal. *11*, eaau0597.

Janic, A., Valente, L.J., Wakefield, M.J., Di Stefano, L., Milla, L., Wilcox, S., Yang, H., Tai, L., Vandenberg, C.J., Kueh, A.J., et al. (2018). DNA repair processes are critical mediators of p53-dependent tumor suppression. Nat. Med. *24*, 947–953.

Jeselsohn, R., Bergholz, J.S., Pun, M., Cornwell, M., Liu, W., Nardone, A., Xiao, T., Li, W., Qiu, X., Buchwalter, G., et al. (2018). Allele-Specific Chromatin Recruitment and Therapeutic Vulnerabilities of ESR1 Activating Mutations. Cancer Cell *33*, 173–186.e5.

Jiang, P., Gu, S., Pan, D., Fu, J., Sahu, A., Hu, X., Li, Z., Traugh, N., Bu, X., Li, B., et al. (2018). Signatures of T cell dysfunction and exclusion predict cancer immunotherapy response. Nat. Med. *24*, 1550–1558.

Kanehisa, M., and Goto, S. (2000). KEGG: kyoto encyclopedia of genes and genomes. Nucleic Acids Res. *28*, 27–30.

Keeshan, K., He, Y., Wouters, B.J., Shestova, O., Xu, L., Sai, H., Rodriguez, C.G., Maillard, I., Tobias, J.W., Valk, P., et al. (2006). Tribbles homolog 2 inactivates C/EBPalpha and causes acute myelogenous leukemia. Cancer Cell *10*, 401–411.

Kim, K., Skora, A.D., Li, Z., Liu, Q., Tam, A.J., Blosser, R.L., Diaz, L.A., Jr., Papadopoulos, N., Kinzler, K.W., Vogelstein, B., and Zhou, S. (2014). Eradication of metastatic mouse cancers resistant to immune checkpoint blockade by suppression of myeloid-derived cells. Proc. Natl. Acad. Sci. USA *111*, 11774–11779.

Ko, C.-Y., Chang, W.-C., and Wang, J.-M. (2015). Biological roles of CCAAT/Enhancer-binding protein delta during inflammation. J. Biomed. Sci. *22*, 6.

Landskron, G., De la Fuente, M., Thuwajit, P., Thuwajit, C., and Hermoso, M.A. (2014). Chronic inflammation and cytokines in the tumor microenvironment. J. Immunol. Res. *2014*, 149185.

Langmead, B., and Salzberg, S.L. (2012). Fast gapped-read alignment with Bowtie 2. Nat. Methods *9*, 357–359.

Lawson, K.A., Sousa, C.M., Zhang, X., Kim, E., Akthar, R., Caumanns, J.J., Yao, Y., Mikolajewicz, N., Ross, C., Brown, K.R., et al. (2020). Functional genomic landscape of cancer-intrinsic evasion of killing by T cells. Nature *586*, 120–126.

Please cite this article in press as: Wang et al., *In vivo* CRISPR screens identify the E3 ligase *Cop1* as a modulator of macrophage infiltration and cancer immunotherapy target, Cell (2021), https://doi.org/10.1016/j.cell.2021.09.006

Li, H., and Durbin, R. (2009). Fast and accurate short read alignment with Burrows-Wheeler transform. Bioinformatics *25*, 1754–1760.

Li, H., Handsaker, B., Wysoker, A., Fennell, T., Ruan, J., Homer, N., Marth, G., Abecasis, G., and Durbin, R.; 1000 Genome Project Data Processing Subgroup (2009). The Sequence Alignment/Map format and SAMtools. Bioinformatics *25*, 2078–2079.

Li, W., Xu, H., Xiao, T., Cong, L., Love, M.I., Zhang, F., Irizarry, R.A., Liu, J.S., Brown, M., and Liu, X.S. (2014). MAGeCK enables robust identification of essential genes from genome-scale CRISPR/Cas9 knockout screens. Genome Biol. *15*, 554.

Li, W., Köster, J., Xu, H., Chen, C.-H., Xiao, T., Liu, J.S., Brown, M., and Liu, X.S. (2015). Quality control, modeling, and visualization of CRISPR screens with MAGeCK-VISPR. Genome Biol. *16*, 281.

Li, B., Severson, E., Pignon, J.-C., Zhao, H., Li, T., Novak, J., Jiang, P., Shen, H., Aster, J.C., Rodig, S., et al. (2016). Comprehensive analyses of tumor immunity: implications for cancer immunotherapy. Genome Biol. *17*, 174.

Li, T., Fan, J., Wang, B., Traugh, N., Chen, Q., Liu, J.S., Li, B., and Liu, X.S. (2017). TIMER: A Web Server for Comprehensive Analysis of Tumor-Infiltrating Immune Cells. Cancer Res. *77*, e108–e110.

Li, L., Liu, Y.-D., Zhan, Y.-T., Zhu, Y.-H., Li, Y., Xie, D., and Guan, X.-Y. (2018). High levels of CCL2 or CCL4 in the tumor microenvironment predict unfavorable survival in lung adenocarcinoma. Thorac. Cancer *9*, 775–784.

Li, S., Wan, C., Zheng, R., Fan, J., Dong, X., Meyer, C.A., and Liu, X.S. (2019). Cistrome-GO: a web server for functional enrichment analysis of transcription factor ChIP-seq peaks. Nucleic Acids Res. *47* (W1), W206–W211.

Li, T., Fu, J., Zeng, Z., Cohen, D., Li, J., Chen, Q., Li, B., and Liu, X.S. (2020). TIMER2.0 for analysis of tumor-infiltrating immune cells. Nucleic Acids Res. *48* (W1), W509–W514.

Lim, S.Y., Yuzhalin, A.E., Gordon-Weeks, A.N., and Muschel, R.J. (2016). Targeting the CCL2-CCR2 signaling axis in cancer metastasis. Oncotarget *7*, 28697–28710.

Love, M.I., Huber, W., and Anders, S. (2014). Moderated estimation of fold change and dispersion for RNA-seq data with DESeq2. Genome Biol. *15*, 550.

Mandal, R., Samstein, R.M., Lee, K.-W., Havel, J.J., Wang, H., Krishna, C., Sabio, E.Y., Makarov, V., Kuo, F., Blecua, P., et al. (2019). Genetic diversity of tumors with mismatch repair deficiency influences anti-PD-1 immunotherapy response. Science *364*, 485–491.

Manguso, R.T., Pope, H.W., Zimmer, M.D., Brown, F.D., Yates, K.B., Miller, B.C., Collins, N.B., Bi, K., LaFleur, M.W., Juneja, V.R., et al. (2017). In vivo CRISPR screening identifies Ptpn2 as a cancer immunotherapy target. Nature *547*, 413–418.

Marine, J.-C. (2012). Spotlight on the role of COP1 in tumorigenesis. Nat. Rev. Cancer *12*, 455–464.

Mei, S., Qin, Q., Wu, Q., Sun, H., Zheng, R., Zang, C., Zhu, M., Wu, J., Shi, X., Taing, L., et al. (2017). Cistrome Data Browser: a data portal for ChIP-Seq and chromatin accessibility data in human and mouse. Nucleic Acids Res. *45* (D1), D658–D662.

Mészáros, B., Kumar, M., Gibson, T.J., Uyar, B., and Dosztányi, Z. (2017). Degrons in cancer. Sci. Signal. *10*, eaak9982.

Meyskens, F.L., Jr., Kopecky, K., Samson, M., Hersh, E., Macdonald, J., Jaffe, H., Crowley, J., and Coltman, C. (1990). Recombinant human interferon gamma: adverse effects in high-risk stage I and II cutaneous malignant melanoma. J. Natl. Cancer Inst. *82*, 1071.

Meyskens, F.L., Jr., Kopecky, K.J., Taylor, C.W., Noyes, R.D., Tuthill, R.J., Hersh, E.M., Feun, L.G., Doroshow, J.H., Flaherty, L.E., and Sondak, V.K. (1995). Randomized trial of adjuvant human interferon gamma versus observation in high-risk cutaneous melanoma: a Southwest Oncology Group study. J. Natl. Cancer Inst. *87*, 1710–1713.

Mezzadra, R., Sun, C., Jae, L.T., Gomez-Eerland, R., de Vries, E., Wu, W., Logtenberg, M.E.W., Slagter, M., Rozeman, E.A., Hofland, I., et al. (2017). Identification of CMTM6 and CMTM4 as PD-L1 protein regulators. Nature *549*, 106–110.

Miao, Z.-H., and Ding, J. (2003). Transcription factor c-Jun activation represses mdr-1 gene expression. Cancer Res. *63*, 4527–4532.

Migliorini, D., Bogaerts, S., Defever, D., Vyas, R., Denecker, G., Radaelli, E., Zwolinska, A., Depaepe, V., Hochepied, T., Skarnes, W.C., and Marine, J.C. (2011). Cop1 constitutively regulates c-Jun protein stability and functions as a tumor suppressor in mice. J. Clin. Invest. *121*, 1329–1343.

Minn, A.J. (2015). Interferons and the Immunogenic Effects of Cancer Therapy. Trends Immunol. *36*, 725–737.

Mootha, V.K., Lindgren, C.M., Eriksson, K.-F., Subramanian, A., Sihag, S., Lehar, J., Puigserver, P., Carlsson, E., Ridderstråle, M., Laurila, E., et al. (2003). PGC-1α-responsive genes involved in oxidative phosphorylation are coordinately downregulated in human diabetes. Nat. Genet. *34*, 267–273.

Motz, G.T., and Coukos, G. (2013). Deciphering and reversing tumor immune suppression. Immunity *39*, 61–73.

Murphy, J.M., Nakatani, Y., Jamieson, S.A., Dai, W., Lucet, I.S., and Mace, P.D. (2015). Molecular Mechanism of CCAAT-Enhancer Binding Protein Recruitment by the TRIB1 Pseudokinase. Structure *23*, 2111–2121.

Nakamae, I., Kato, J.-Y., Yokoyama, T., Ito, H., and Yoneda-Kato, N. (2017). Myeloid leukemia factor 1 stabilizes tumor suppressor C/EBPα to prevent Trib1-driven acute myeloid leukemia. Blood Adv. *1*, 1682–1693.

Nanda, R., Chow, L.Q.M., Dees, E.C., Berger, R., Gupta, S., Geva, R., Pusztai, L., Pathiraja, K., Aktan, G., Cheng, J.D., et al. (2016). Pembrolizumab in Patients With Advanced Triple-Negative Breast Cancer: Phase Ib KEYNOTE-012 Study. J. Clin. Oncol. *34*, 2460–2467.

Ndoja, A., Reja, R., Lee, S.-H., Webster, J.D., Ngu, H., Rose, C.M., Kirkpatrick, D.S., Modrusan, Z., Chen, Y.-J.J., Dugger, D.L., et al. (2020). Ubiquitin Ligase COP1 Suppresses Neuroinflammation by Degrading c/EBPβ in Microglia. Cell *182*, 1156–1169.e12.

Newman, A.M., Liu, C.L., Green, M.R., Gentles, A.J., Feng, W., Xu, Y., Hoang, C.D., Diehn, M., and Alizadeh, A.A. (2015). Robust enumeration of cell subsets from tissue expression profiles. Nat. Methods *12*, 453–457.

Newman, A.M., Steen, C.B., Liu, C.L., Gentles, A.J., Chaudhuri, A.A., Scherer, F., Khodadoust, M.S., Esfahani, M.S., Luca, B.A., Steiner, D., et al. (2019). Determining cell type abundance and expression from bulk tissues with digital cytometry. Nat. Biotechnol. *37*, 773–782.

Nielsen, S.R., and Schmid, M.C. (2017). Macrophages as Key Drivers of Cancer Progression and Metastasis. Mediators Inflamm. *2017*, 9624760.

Noy, R., and Pollard, J.W. (2014). Tumor-associated macrophages: from mechanisms to therapy. Immunity *41*, 49–61.

Nusinow, D.P., Szpyt, J., Ghandi, M., Rose, C.M., McDonald, E.R., 3rd, Kalocsay, M., Jané-Valbuena, J., Gelfand, E., Schweppe, D.K., Jedrychowski, M., et al. (2020). Quantitative Proteomics of the Cancer Cell Line Encyclopedia. Cell *180*, 387–402.e16.

Osterlund, M.T., Hardtke, C.S., Wei, N., and Deng, X.W. (2000). Targeted destabilization of HY5 during light-regulated development of Arabidopsis. Nature *405*, 462–466.

Pan, D., Kobayashi, A., Jiang, P., Ferrari de Andrade, L., Tay, R.E., Luoma, A.M., Tsoucas, D., Qiu, X., Lim, K., Rao, P., et al. (2018). A major chromatin regulator determines resistance of tumor cells to T cell-mediated killing. Science *359*, 770–775.

Patro, R., Duggal, G., Love, M.I., Irizarry, R.A., and Kingsford, C. (2017). Salmon provides fast and bias-aware quantification of transcript expression. Nat. Methods *14*, 417–419.

Pearlman, R., Frankel, W.L., Swanson, B., Zhao, W., Yilmaz, A., Miller, K., Bacher, J., Bigley, C., Nelsen, L., Goodfellow, P.J., et al.; Ohio Colorectal Cancer Prevention Initiative Study Group (2017). Prevalence and Spectrum of Germline Cancer Susceptibility Gene Mutations Among Patients With Early-Onset Colorectal Cancer. JAMA Oncol. *3*, 464–471.

Peranzoni, E., Lemoine, J., Vimeux, L., Feuillet, V., Barrin, S., Kantari-Mimoun, C., Bercovici, N., Guérin, M., Biton, J., Ouakrim, H., et al. (2018). Macrophages impede CD8 T cells from reaching tumor cells and limit the efficacy of anti-PD-1 treatment. Proc. Natl. Acad. Sci. USA *115*, E4041–E4050.

Please cite this article in press as: Wang et al., *In vivo* CRISPR screens identify the E3 ligase *Cop1* as a modulator of macrophage infiltration and cancer immunotherapy target, Cell (2021), https://doi.org/10.1016/j.cell.2021.09.006

Qian, B.-Z., Li, J., Zhang, H., Kitamura, T., Zhang, J., Campion, L.R., Kaiser, E.A., Snyder, L.A., and Pollard, J.W. (2011). CCL2 recruits inflammatory monocytes to facilitate breast-tumour metastasis. Nature *475*, 222–225.

Qin, Q., Mei, S., Wu, Q., Sun, H., Li, L., Taing, L., Chen, S., Li, F., Liu, T., Zang, C., et al. (2016). ChiLin: a comprehensive ChIP-seq and DNase-seq quality control and analysis pipeline. BMC Bioinformatics *17*, 404.

Qin, Q., Fan, J., Zheng, R., Wan, C., Mei, S., Wu, Q., Sun, H., Brown, M., Zhang, J., Meyer, C.A., and Liu, X.S. (2020). Lisa: inferring transcriptional regulators through integrative modeling of public chromatin accessibility and ChIP-seq data. Genome Biol. *21*, 32.

Quinlan, A.R., and Hall, I.M. (2010). BEDTools: a flexible suite of utilities for comparing genomic features. Bioinformatics *26*, 841–842.

Racle, J., de Jonge, K., Baumgaertner, P., Speiser, D.E., and Gfeller, D. (2017). Simultaneous enumeration of cancer and immune cell types from bulk tumor gene expression data. eLife *6*, e26476.

Ramilowski, J.A., Goldberg, T., Harshbarger, J., Kloppmann, E., Lizio, M., Satagopam, V.P., Itoh, M., Kawaji, H., Carninci, P., Rost, B., and Forrest, A.R. (2015). A draft network of ligand-receptor-mediated multicellular signalling in human. Nat. Commun. *6*, 7866.

Ramírez, F., Ryan, D.P., Grüning, B., Bhardwaj, V., Kilpert, F., Richter, A.S., Heyne, S., Dündar, F., and Manke, T. (2016). deepTools2: a next generation web server for deep-sequencing data analysis. Nucleic Acids Res. *44* (W1), W160-5.

Ritchie, M.E., Phipson, B., Wu, D., Hu, Y., Law, C.W., Shi, W., and Smyth, G.K. (2015). limma powers differential expression analyses for RNA-sequencing and microarray studies. Nucleic Acids Res. *43*, e47.

Sagiv-Barfi, I., Kohrt, H.E.K., Czerwinski, D.K., Ng, P.P., Chang, B.Y., and Levy, R. (2015). Therapeutic antitumor immunity by checkpoint blockade is enhanced by ibrutinib, an inhibitor of both BTK and ITK. Proc. Natl. Acad. Sci. USA *112*, E966–E972.

Satoh, T., Kidoya, H., Naito, H., Yamamoto, M., Takemura, N., Nakagawa, K., Yoshioka, Y., Morii, E., Takakura, N., Takeuchi, O., and Akira, S. (2013). Critical role of Trib1 in differentiation of tissue-resident M2-like macrophages. Nature *495*, 524–528.

Savio, M.G., Rotondo, G., Maglie, S., Rossetti, G., Bender, J.R., and Pardi, R. (2008). COP1D, an alternatively spliced constitutive photomorphogenic-1 (COP1) product, stabilizes UV stress-induced c-Jun through inhibition of full-length COP1. Oncogene *27*, 2401–2411.

Schmid, P., Adams, S., Rugo, H.S., Schneeweiss, A., Barrios, C.H., Iwata, H., Diéras, V., Hegg, R., Im, S.-A., Shaw Wright, G., et al.; IMpassion130 Trial Investigators (2018). Atezolizumab and Nab-Paclitaxel in Advanced Triple-Negative Breast Cancer. N. Engl. J. Med. *379*, 2108–2121.

Seo, H.S., Yang, J.-Y., Ishikawa, M., Bolle, C., Ballesteros, M.L., and Chua, N.-H. (2003). LAF1 ubiquitination by COP1 controls photomorphogenesis and is stimulated by SPA1. Nature *423*, 995–999.

Singh, A.A., Schuurman, K., Nevedomskaya, E., Stelloo, S., Linder, S., Droog, M., Kim, Y., Sanders, J., van der Poel, H., Bergman, A.M., Wessels, L.F., and Zwart, W. (2018). Optimized ChIP-seq method facilitates transcription factor profiling in human tumors. Life science alliance *2* (1), e201800115.

Stuart, T., Butler, A., Hoffman, P., Hafemeister, C., Papalexi, E., Mauck, W.M., 3rd, Hao, Y., Stoeckius, M., Smibert, P., and Satija, R. (2019). Comprehensive Integration of Single-Cell Data. Cell *177*, 1888–1902.e21.

Sturm, G., Finotello, F., Petitprez, F., Zhang, J.D., Baumbach, J., Fridman, W.H., List, M., and Aneichyk, T. (2019). Comprehensive evaluation of transcriptome-based cell-type quantification methods for immuno-oncology. Bioinformatics *35*, i436–i445.

Su, S., Chen, J., Yao, H., Liu, J., Yu, S., Lao, L., Wang, M., Luo, M., Xing, Y., Chen, F., et al. (2018). $CD10^{+}GPR77^{+}$ Cancer-Associated Fibroblasts Promote Cancer Formation and Chemoresistance by Sustaining Cancer Stemness. Cell *172*, 841–856.e16.

Sun, H., Lu, J., Liu, L., Yang, C.Y., and Wang, S. (2014). Potent and selective small-molecule inhibitors of cIAP1/2 proteins reveal that the binding of Smac mimetics to XIAP BIR3 is not required for their effective induction of cell death in tumor cells. ACS Chem. Biol. *9*, 994–1002.

Tisato, V., Voltan, R., Gonelli, A., Secchiero, P., and Zauli, G. (2017). MDM2/X inhibitors under clinical evaluation: perspectives for the management of hematological malignancies and pediatric cancer. J. Hematol. Oncol. *10*, 133.

Tsherniak, A., Vazquez, F., Montgomery, P.G., Weir, B.A., Kryukov, G., Cowley, G.S., Gill, S., Harrington, W.F., Pantel, S., Krill-Burger, J.M., et al. (2017). Defining a Cancer Dependency Map. Cell *170*, 564–576.e16.

UniProt Consortium (2019). UniProt: a worldwide hub of protein knowledge. Nucleic Acids Res. *47* (D1), D506–D515.

Vitari, A.C., Leong, K.G., Newton, K., Yee, C., O'Rourke, K., Liu, J., Phu, L., Vij, R., Ferrando, R., Couto, S.S., et al. (2011). COP1 is a tumour suppressor that causes degradation of ETS transcription factors. Nature *474*, 403–406.

Wachter, F., Morgan, A.M., Godes, M., Mourtada, R., Bird, G.H., and Walensky, L.D. (2017). Mechanistic validation of a clinical lead stapled peptide that reactivates p53 by dual HDM2 and HDMX targeting. Oncogene *36*, 2184–2190.

Waks, A.G., and Winer, E.P. (2019). Breast Cancer Treatment. JAMA *321*, 316.

Walens, A., DiMarco, A.V., Lupo, R., Kroger, B.R., Damrauer, J.S., and Alvarez, J.V. (2019). CCL5 promotes breast cancer recurrence through macrophage recruitment in residual tumors. eLife *8*, e43653.

Wang, D., Sun, H., Wei, J., Cen, B., and DuBois, R.N. (2017). CXCL1 Is Critical for Premetastatic Niche Formation and Metastasis in Colorectal Cancer. Cancer Res. *77*, 3655–3665.

Wang, B., Wang, M., Zhang, W., Xiao, T., Chen, C.-H., Wu, A., Wu, F., Traugh, N., Wang, X., Li, Z., et al. (2019). Integrative analysis of pooled CRISPR genetic screens using MAGeCKFlute. Nat. Protoc. *14*, 756–780.

Wang, C., Sun, D., Huang, X., Wan, C., Li, Z., Han, Y., Qin, Q., Fan, J., Qiu, X., Xie, Y., et al. (2020). Integrative analyses of single-cell transcriptome and regulome using MAESTRO. Genome Biol. *21*, 198.

Wehde, B.L., Rädler, P.D., Shrestha, H., Johnson, S.J., Triplett, A.A., and Wagner, K.-U. (2018). Janus Kinase 1 Plays a Critical Role in Mammary Cancer Progression. Cell Rep. *25*, 2192–2207.e5.

Wei, W., and Kaelin, W.G., Jr. (2011). Good COP1 or bad COP1? In vivo veritas. J. Clin. Invest. *121*, 1263–1265.

Wertz, I.E., O'Rourke, K.M., Zhang, Z., Dornan, D., Arnott, D., Deshaies, R.J., and Dixit, V.M. (2004). Human De-etiolated-1 regulates c-Jun by assembling a CUL4A ubiquitin ligase. Science *303*, 1371–1374.

Wong, W.C., Kim, D., Carter, H., Diekhans, M., Ryan, M.C., and Karchin, R. (2011). CHASM and SNVBox: toolkit for detecting biologically important single nucleotide mutations in cancer. Bioinformatics *27*, 2147–2148.

Xiao, T., Li, W., Wang, X., Xu, H., Yang, J., Wu, Q., Huang, Y., Geradts, J., Jiang, P., Fei, T., et al. (2018). Estrogen-regulated feedback loop limits the efficacy of estrogen receptor-targeted breast cancer therapy. Proc. Natl. Acad. Sci. USA *115*, 7869–7878.

Xu, H., Xiao, T., Chen, C.-H., Li, W., Meyer, C.A., Wu, Q., Wu, D., Cong, L., Zhang, F., Liu, J.S., et al. (2015). Sequence determinants of improved CRISPR sgRNA design. Genome Res. *25*, 1147–1157.

Xu, W., Zhong, Q., Lin, D., Li, G., and Cao, G. (2021). CoolBox: A flexible toolkit for visual analysis of genomics data. bioRxiv. https://doi.org/10.1101/2021.04.15.439923.

Yu, G., Wang, L.-G., Han, Y., and He, Q.-Y. (2012). clusterProfiler: an R package for comparing biological themes among gene clusters. OMICS *16*, 284–287.

Zhang, Y., Liu, T., Meyer, C.A., Eeckhoute, J., Johnson, D.S., Bernstein, B.E., Nusbaum, C., Myers, R.M., Brown, M., Li, W., and Liu, X.S. (2008). Model-based analysis of ChIP-Seq (MACS). Genome Biol. *9*, R137.

Zhang, J., Yan, Y., Yang, Y., Wang, L., Li, M., Wang, J., Liu, X., Duan, X., and Wang, J. (2016). High Infiltration of Tumor-Associated Macrophages Influences Poor Prognosis in Human Gastric Cancer Patients, Associates With the Phenomenon of EMT. Medicine (Baltimore) *95*, e2636.

Please cite this article in press as: Wang et al., *In vivo* CRISPR screens identify the E3 ligase *Cop1* as a modulator of macrophage infiltration and cancer immunotherapy target, Cell (2021), https://doi.org/10.1016/j.cell.2021.09.006

Zhang, X., Crowley, V.M., Wucherpfennig, T.G., Dix, M.M., and Cravatt, B.F. (2019). Electrophilic PROTACs that degrade nuclear proteins by engaging DCAF16. Nat. Chem. Biol. *15*, 737–746.

Zhao, J., Ou, B., Han, D., Wang, P., Zong, Y., Zhu, C., Liu, D., Zheng, M., Sun, J., Feng, H., and Lu, A. (2017). Tumor-derived CXCL5 promotes human colorectal cancer metastasis through activation of the ERK/Elk-1/Snail and AKT/GSK3β/β-catenin pathways. Mol. Cancer *16*, 70.

Zheng, R., Wan, C., Mei, S., Qin, Q., Wu, Q., Sun, H., Chen, C.-H., Brown, M., Zhang, X., Meyer, C.A., and Liu, X.S. (2019). Cistrome Data Browser: expanded datasets and new tools for gene regulatory analysis. Nucleic Acids Res. *47* (D1), D729–D735.

Please cite this article in press as: Wang et al., *In vivo* CRISPR screens identify the E3 ligase *Cop1* as a modulator of macrophage infiltration and cancer immunotherapy target, Cell (2021), https://doi.org/10.1016/j.cell.2021.09.006

STAR★METHODS

KEY RESOURCES TABLE

REAGENT or RESOURCE	SOURCE	IDENTIFIER
Antibodies		
Rabbit monoclonal anti-mouse/human Cop1	Bethyl	Cat# A300-894A, RRID:AB_625290
Rabbit monoclonal anti-mouse/human PD-L1	Thermo Fisher Scientific	Cat# PA5-20343, RRID:AB_11153819
IgG2a Isotype control	Bio X Cell	Cat# BE0089, RRID:AB_1107769
Rabbit monoclonal anti-mouse/human p53	Cell Signaling Technology	Cat# 9282, RRID:AB_331476
Mouse monoclonal anti-human ER	Cell Signaling Technology	Cat# 2512, RRID:AB_331291
Rabbit monoclonal anti-human/mouse PR	Cell Signaling Technology	Cat# 3153, RRID:AB_1031219
Mouse monoclonal anti-human HER2	Santa Cruz Biotechnology	Cat# sc-33684, RRID:AB_627996
Rabbit monoclonal anti-human/mouse GAPDH	Cell Signaling Technology	Cat# 5174, RRID:AB_10622025
Rabbit monoclonal anti-human/mouse STAT1	Cell Signaling Technology	Cat# 14994, RRID:AB_2737027
Rabbit monoclonal anti-human/mouse JAK1	Cell Signaling Technology	Cat# 3344, RRID:AB_2265054
Rabbit monoclonal anti-human/mouse C/EBPδ	Abcam	Cat#ab245214
Rabbit monoclonal anti-human/mouse TRIB2	Cell Signaling Technology	Cat# 13533, RRID:AB_2798250
Rabbit monoclonal anti-human/mouse C/EBPα	Cell Signaling Technology	Cat# 8178, RRID:AB_11178517
Goat anti-Mouse IgG Secondary Antibody, HRP	Thermo Fisher Scientific	Cat# 31430, RRID:AB_228307
Donkey anti-Rabbit IgG Secondary Antibody, HRP	Thermo Fisher Scientific	Cat# 31458, RRID:AB_228213
Ly-6C antibody	BD Biosciences	Cat# 562727, RRID:AB_2737748
FITC anti-mouse CD206	BioLegend	Cat# 141703, RRID:AB_10900988
PE anti-mouse/human CD11b antibody	BioLegend	Cat# 101207, RRID:AB_312790
PE/Cyanine7 anti-mouse Ly-6G antibody	BioLegend	Cat# 127617, RRID:AB_1877262
CD11c antibody	BD Biosciences	Cat# 561119, RRID:AB_10562405
APC/Cyanine7 anti-mouse CD45.2 antibody	BioLegend	Cat# 109823, RRID:AB_830788
Brilliant Violet 421(TM) anti-mouse CD335 (NKp46) antibody	BioLegend	Cat# 137612, RRID:AB_2563104
Brilliant Violet 510(TM) anti-mouse CD62L antibody	BioLegend	Cat# 104441, RRID:AB_2561537
Brilliant Violet 605(TM) anti-mouse/human CD44 antibody	BioLegend	Cat# 103047, RRID:AB_2562451
Brilliant Violet 711(TM) anti-mouse CD8a antibody	BioLegend	Cat# 100747, RRID:AB_11219594
Rat Anti-Mouse CD49b / Pan-NK Cells Monoclonal Antibody	BD Biosciences	Cat# 561067, RRID:AB_2034010
PE anti-mouse CD45.2 antibody	BioLegend	Cat# 109807, RRID:AB_313444
PE/Cyanine7 anti-mouse TCR beta chain antibody	BioLegend	Cat# 109221, RRID:AB_893627
APC/Cyanine7 anti-mouse CD4 antibody	BioLegend	Cat# 100413, RRID:AB_312698
I-A/I-E antibody	BD Biosciences	Cat# 563414, RRID:AB_2738191
APC anti-mouse CD19 antibody	BioLegend	Cat# 115511, RRID:AB_313646
Experimental models: Cell lines		
Human: HEK293FT	Thermo Fisher Scientific	Cat#R70007
Human: MCF-7	American Type Culture Collection	Cat# HTB-22, RRID:CVCL_0031
Human: T47D	American Type Culture Collection	Cat# HTB-133, RRID:CVCL_0553
Mouse: 4T1	American Type Culture Collection	Cat# CRL-2539, RRID:CVCL_0125
Mouse: EMT6	American Type Culture Collection	Cat# CRL-2755, RRID:CVCL_1923
Mouse: 246	Myles Brown Lab	N/A
Mouse: JC	American Type Culture Collection	Cat# CRL-2116, RRID:CVCL_3530
Mouse: MC38	Kai Wucherpfennig Lab	N/A

(*Continued on next page*)

Please cite this article in press as: Wang et al., *In vivo* CRISPR screens identify the E3 ligase *Cop1* as a modulator of macrophage infiltration and cancer immunotherapy target, Cell (2021), https://doi.org/10.1016/j.cell.2021.09.006

Continued

REAGENT or RESOURCE	SOURCE	IDENTIFIER
Experimental models: Organisms/strains		
Mouse: BALB/c	IMSR	Cat# CRL:028, RRID:IMSR_CRL:028
Mouse: BALB/c Foxn1nu/nu	IMSR	Cat# CRL:194, RRID:IMSR_CRL:194
Mouse: C57BL/6	IMSR	Cat# JAX:000664, RRID:IMSR_JAX:000664
Mouse: C57BL/6 Foxn1nu/nu	IMSR	Cat# JAX:000819, RRID:IMSR_JAX:000819
Bacterial and virus strains		
XL10-Gold Ultracompetent Cells	Agilent	Cat# 200314
Endura ElectroCompetent Cells	Lucigen	Cat# 60242-2
Chemicals, peptides, and recombinant proteins		
PBS	GIBCO	Cat# 14190250
DMEM, high glucose, pyruvate	GIBCO	Cat# 11995065
Lonza BioWhittaker L-Glutamine (200mM)	Lonza	Cat# BW17605E
Fetal bovine serum	VWR	Cat# 9706
Penicillin-Streptomycin	GIBCO	Cat# 15140122
E-Gel Low Range Quantitative DNA Ladder	Invitrogen	Cat# NP0008
E-Gel EX Agarose Gels, 2%	Life Technologies	Cat# G402002
NuPAGE 3-8% Tris-Acetate Protein Gels, 1.5 mm, 10-well	Life Technologies	Cat# EA0378BOX
NuPAGE LDS Sample Buffer	Life Technologies	Cat# NP0008
Pierce ECL Western Blotting Substrate	Thermo Fisher Scientific	Cat# 32106
Precision Plus Protein Dual Color Standards	Bio-Rad Laboratories	Cat# 161-0394
X-tremeGENE HP DNA Transfection Reagent	Sigma-Aldrich	Cat# 6366236001
Polybrene	Sigma-Aldrich	Cat# 107689-10G
Puromycin dihydrochloride	Thermo Fisher Scientific	Cat# A1113803
BamHI-HF	New England Biolabs	Cat# R3136S
EcoRI-HF	New England Biolabs	Cat# R3101S
FastDigest Esp3I	Thermo Fisher Scientific	Cat# FD0454
Q5 DNA Polymerase	New England Biolabs	Cat# M0491L
Nuclease-Free Water	Ambion	Cat# AM9938
Pierce Homobifunctional Cross Linkers	Life Technologies	Cat# 20593
2-Mercaptoethanol	Sigma Aldrich	Cat# M6250-10ML
Dynabeads Protein A	Thermo Fisher Scientific	Cat# 10004D
Dynabeads Protein G	Thermo Fisher Scientific	Cat# 10002D
EDTA	Sigma Aldrich	Cat# E8008-100ML
Protease/Phosphatase Inhibitor Cocktail (100X)	Cell Signaling Technology	Cat# 5872S
Quick-Load 1 kb Plus DNA Ladder	New England Biolabs	Cat# N0469S
LB Broth	Mp Biomedicals	Cat# 244610
L-Broth Agar Large Capsules	Mp Biomedicals	Cat# MP 113001236
RIPA buffer	Invitrogen	Cat# R0278
Pierce 16% Formaldehyde (w/v), Methanol-free	Life Technologies	Cat# 28906
Opti-MEM I Reduced Serum Medium, no phenol red	Thermo Fisher Scientific	Cat# 11058021
Critical commercial assays		
QIAprep Spin Miniprep Kit	QIAGEN	Cat# 27106
RNeasy Plus Mini Kit	QIAGEN	Cat# 74134
QIAquick PCR Purification Kit	QIAGEN	Cat# 28104
QIAquick gel extraction kit	QIAGEN	Cat# 28704

(*Continued on next page*)

Please cite this article in press as: Wang et al., *In vivo* CRISPR screens identify the E3 ligase *Cop1* as a modulator of macrophage infiltration and cancer immunotherapy target, Cell (2021), https://doi.org/10.1016/j.cell.2021.09.006

Continued

REAGENT or RESOURCE	SOURCE	IDENTIFIER
Gibson Assembly Master Mix	New England Biolabs	Cat# E2611L
iScript cDNA Synthesis Kit	Bio-Rad Laboratories	Cat# 1708891
SsoAdvanced Univ SYBR Grn Suprmx	Bio-Rad Laboratories	Cat# 1725272
Qubit dsDNA HS Assay Kit	Thermo Fisher Scientific	Cat# Q32854
Qubit RNA HS Assay Kit	Thermo Fisher Scientific	Cat# Q32855
GenElute HP Plasmid Maxiprep Kit	Sigma-Aldrich	Cat# NA0410-1KT
Ampure xp	Beckman Coulter	Cat# A63881
Mouse Cytokine Array	RayBiotech	Cat# C1000
BCA Assay Kit	Thermo Fisher Scientific	Cat# 23225
SMARTer® ThruPLEX® DNA-Seq Kit	Takara Bio	Cat# R400675
Oligonucleotides		
MusCK oligo pool	Twist bioscience	N/A
MusCK2.0 oligo pool	Twist bioscience	N/A
Primers for knockout or real-time PCR, see Data and code availability	This paper	N/A
Recombinant DNA		
lentiCRISPR v2 blast	Addgene	RRID:Addgene_83480
lentiCRISPR v2 puro	Addgene	RRID:Addgene_98290
pMD2.G	Addgene	RRID:Addgene_12259
psPAX2	Addgene	RRID:Addgene_12260
pCI-neo-sOVA	Addgene	RRID:Addgene_25098
pCI-neo-mOVA	Addgene	RRID:Addgene_25099
pCI-neo-cOVA	Addgene	RRID:Addgene_25097
pcDNA3-OVA	Addgene	RRID:Addgene_64599
lentiV2-blast-sOva	This paper	N/A
lentiV2-blast-mOva	This paper	N/A
lentiV2-blast-cOva	This paper	N/A
lentiV2-blast-Ova	This paper	N/A
pLentiCRISPR-EGFP	Addgene	RRID:Addgene_75159
pEF1A-puro	This paper	N/A
pLentiCRISPR-mCherry	Addgene	RRID:Addgene_75161
Software and algorithms		
GraphPad Prism 7	GraphPad Software	https://www.graphpad.com
GSEA	Mootha et al., 2003	https://www.gsea-msigdb.org/gsea/msigdb/annotate.jsp
Flow Jo_v10	FlowJo	https://www.flowjo.com/
BWA	Li and Durbin, 2009	https://github.com/lh3/bwa
CoolBox	Xu et al., 2021	https://github.com/GangCaoLab/CoolBox
Bowtie2	Langmead and Salzberg, 2012	http://bowtie-bio.sourceforge.net/bowtie2/index.shtml
LISA	Qin et al., 2020	http://cistrome.org
Cistrome-GO	Li et al., 2019	http://go.cistrome.org
LIMMA	Ritchie et al., 2015	https://bioconductor.org/packages/release/bioc/html/limma.html
Samtools	Li et al., 2009	http://samtools.sourceforge.net/
Deposited data		
Data files for RNA-seq (processed data)	This paper	The NCBI GEO database (GSE171467, GSE173296)

(*Continued on next page*)

Please cite this article in press as: Wang et al., *In vivo* CRISPR screens identify the E3 ligase *Cop1* as a modulator of macrophage infiltration and cancer immunotherapy target, Cell (2021), https://doi.org/10.1016/j.cell.2021.09.006

Continued

REAGENT or RESOURCE	SOURCE	IDENTIFIER
Data files for ATAC-seq (processed data)	This paper	The NCBI GEO database (GSE174784)
Data files for ChIP-seq (processed data)	This paper	The NCBI GEO database (GSE175332)
Primer sequence	This paper	https://data.mendeley.com/datasets/9d5499gb8x/1
Code	This paper	https://github.com/liulab-dfci/Cop1_Cell_2021
Other		
Corning Filter System (0.45um)	Corning Life Sciences	Cat# 431096
milliTUBE 1 ml AFA Fiber	Covaris Inc.	Cat# 520130
NITROCEL MEMB 0.45um	Bio-Rad Laboratories	Cat# 1620115
Multiplate 96-Well PCR Plates	Bio-Rad Laboratories	Cat# MLL9601
QUBIT ASSAY TUBES SET	Life Technologies	Cat# Q32856
Microseal B Adhesive Seals	Bio-Rad Laboratories	Cat# MSB-1001

RESOURCE AVAILABILITY

Lead contact

Further information and requests for resources (including code) should be directed to and will be fulfilled by the Lead Contact, X. Shirley Liu (xsliu@ds.dfci.harvard.edu).

Materials availability

Further information and requests for reagents may be directed to, and will be fulfilled by Dr. Myles Brown (Myles_Brown@DFCI.harvard.edu). A list of critical reagents (key resources) is included in the Key resources table. Relevant plasmids are available to the academic community. For additional materials, please email the lead contact for requests. Some material may require requests to collaborators and/or agreements with various entities. Requests are reviewed by DFCI regarding intellectual property or confidentiality obligations. Material that can be shared will be released via a Material Transfer Agreement.

Data and code availability

The processed sequencing data in this paper have been deposited into the NCBI GEO database: GSE171467, GSE173296, GSE174784, GSE175332. Additional Supplemental Items are available at Mendeley Data: https://data.mendeley.com/datasets/9xkgn447vz/1; https://data.mendeley.com/datasets/9d5499gb8x/1. All the code are also available at GitHub: https://github.com/liulab-dfci/Cop1_Cell_2021.

EXPERIMENTAL MODEL AND SUBJECT DETAILS

Mice

All animal experiments were approved by the Institutional Animal Care and Use Committee (IACUC) of Dana Farber Cancer Institute (DFCI) and performed with approved protocol (16-005). Six to eight week old female BALB/c (Stock# 028) and BALB/c Foxn1$^{nu/nu}$ (Stock# 194) were obtained from Charles River Laboratory (Wilmington, MA). Six to eight week old female C57BL/6 (Stock# 000664) and C57BL/6 Foxn1$^{nu/nu}$ (Stock# 000819) were obtained from Jackson Laboratory (Bar Harbor, ME). All animals were housed in standard individually ventilated, pathogen-free conditions, with 12h: 12h light cycle, room temperature (21-23°C) and 40%–60% relative humidity. When a cohort of animals were receiving multiple treatments, animals were randomized by 1) randomly assign animals to different groups using littermates, 2) random mixing of mice prior to treatment, maximizing the evenness or representation of mice from different cages in each group, and/or 3) random assignment of mice to each group, in order to minimize the effect of gender, litter, small difference in age, cage, housing position, where applicable. Average tumor sizes were consistent between treatment groups to account for selection bias.

Cell Lines

Murine 4T1, EMT6, JC breast cancer cells were obtained from American Type Culture Collection (ATCC) and cultured according to standard protocols. MCF7 and T47D human breast cancer cells were derived and cultured as previously described (Xiao et al., 2018). MC38 murine colon adenocarcinoma cells were obtained from Kai Wucherpfennig laboratory.

Please cite this article in press as: Wang et al., *In vivo* CRISPR screens identify the E3 ligase *Cop1* as a modulator of macrophage infiltration and cancer immunotherapy target, Cell (2021), https://doi.org/10.1016/j.cell.2021.09.006

METHOD DETAILS

Large-scale mouse CRISPR library cloning

SgRNA design primarily targeted low G-C content regions of the genome. We assigned predicted performance scores to all possible sgRNAs targeting each gene, and selected top candidate sgRNAs with the highest predicted on-target KO efficiency and lowest off-target efficiency (Chen et al., 2018a; Xu et al., 2015). Customized single-stranded oligonucleotide pools of CRISPR guide RNA (sgRNA) libraries were synthesized by Twist Bioscience (South San Francisco, CA). The double-stranded oligonucleotides were generated by polymerase chain reaction and cloned into lentiviral CRISPR vector (lentiCRISPR-v2-puro) by Gibson assembly at estimated equal molar ratios to generate the large-scale mouse CRISPR library (MusCK and MusCK 2.0 libraries). The MusCK library consisted of 24,622 sgRNAs including 1,000 non-targeting controls (NTCs) and 23,622 unique sgRNAs targeting 4,787 gene locations in the genome. The MusCK 2.0 library consisted of 800 sgRNAs including 168 non-targeting controls (NTCs) and 632 unique sgRNAs targeting 79 gene locations in the genome. We were aware that in large-scale CRISPR screen efforts, the statistical power of discovery is particularly sensitive to the behavioral consistency of multiple sgRNAs for each target gene. ''Outlier'' behavior (extreme depletion or enrichment) of one sgRNA out of all sgRNAs targeting the same gene could result in a false positive result. We recognize that the CRISPR KO libraries designed by the Broad Institute are so far the most widely accepted in genomic screen studies; thus, we wanted to ensure that our findings by the MusCK library are reproducible when the Broad sgRNA design principles were applied. To this end, in the MusCK 2.0 library, eight sgRNAs (four designed by our group in MusCK, another four referenced from the Broad Institute's Brie Mouse CRISPR Knockout Pool Library) (Doench et al., 2016) were designated to each candidate gene. An estimated library coverage of ~300X (total colonies / sgRNAs) was achieved by electroporation. These libraries were subsequently sequence-verified by Illumina sequencing to ensure the high quality of sgRNA distribution.

Viral library production

The CRISPR library plasmids were transfected into HEK293FT cells at 90% confluence in 15cm tissue culture plates. Viral supernatant was collected at 48 hours and 72 hours post-transfection, filtered via a 0.45 μm filtration unit (Corning, Cat# 430770). The supernatant was subsequently aliquoted and stored in −80°C freezer until use.

Viral transduction of cancer cells

Cancer cells were cultured according to standard protocols. Similar to our previous studies (Fei et al., 2017; Xiao et al., 2018), for the pooled large-scale CRISPR screen, a total of $> 1 \times 10^8$ cancer cells were transduced with lentivirus containing the library described above at a multiplicity of infection (MOI) of ~0.3. After puromycin selection for 3 days, ~30% of the surviving cells were stored as Day-0-input samples at −80°C, and the rest of cells were cultured for *in vitro* or *in vivo* screenings. PCR of the regions targeted by the library was performed on genomic DNA to construct the sequencing library. Each library was sequenced at ~30 million reads to achieve ~300-fold coverage over the CRISPR library. Sequencing data were analyzed by using MAGeCK and MAGeCK-VISPR (Li et al., 2014, 2015; Wang et al., 2019).

Genomic DNA extraction

For genomic DNA extraction, two methods were used. Method 1: for cellular samples with a total number greater than 3×10^7 cells, or tumor samples from mice, a custom DNA extraction protocol was used. Briefly, frozen tumors were disrupted on dry ice, then resuspended in 7 mL of Lysis Buffer (400 mM Sodium chloride 10 mM Tris, 2 mM EDTA, 0.5% SDS, pH 8) in a 15 mL conical tube, and 80 μL of 20 mg/ml Proteinase K (Invitrogen) were added to the tumor/cell samples and incubated at 55°C for at least 6 hours. The next day, 80 μL of 20 mg/ml RNase A (Invitrogen) was added to the lysed sample, which was then inverted 10 times and incubated at 65°C for 60 minutes. Samples were cooled on ice before addition of 7 mL of pre-chilled phenol/chloroform (Ambion) to precipitate proteins. The samples were vortexed at high speed for 20 s and then centrifuged at 14,000 rpm for 10 minutes. Then, the upper aqueous phase was carefully decanted into a new 15 mL conical tube. Then 7 mL freshly prepared 70% ethanol was added to the tube, vortexed at high speed for 20 s and centrifuged at 12,000 rpm for 10 minutes. Genomic DNA was visible as a small white pellet in each tube. The supernatant was discarded, 6 mL of 70% ethanol was added, the tube was inverted 10 times, and then centrifuged at 12,000 rpm for 5 minutes. The supernatant was discarded by pouring; the tube was briefly spun, and remaining ethanol was removed using a P200 pipette. After air-drying for more than 30 minutes, the DNA changed appearance from a milky white pellet to slightly translucent. Then, 500 μL of nuclease-free water was added, the tube was incubated at 4°C overnight to fully resuspend the DNA. The next day, the gDNA samples were vortexed briefly. The gDNA concentration was measured using a Nanodrop (Thermo Scientific). Method 2: for cellular samples with a total number $< 1 \times 10^7$ cells, samples were subjected to Allprep DNA/RNA Mini Kit (QIAGEN) following the manufacturer's protocol.

sgRNA library readout by deep sequencing

The sgRNA library readout was performed using a two-steps PCR strategy, where the first PCR includes enough genomic DNA to preserve full library complexity and the second PCR adds appropriate sequencing adapters to the products from the first PCR.

For PCR#1, a region containing sgRNA cassette was amplified using primers specific to the lentiCRISPR-v2 vector (Primers for sequencing library construction, see Data and code availability). PCR was performed using Q5 High-Fidelity DNA Polymerase (NEB). For reactions using Q5 High-Fidelity DNA Polymerase, in PCR#1, the thermocycling parameters were:

STEP	TEMP	TIME
Initial Denaturation	98°C	30 s
18 Cycles	98°C	15 s
	68°C	25 s
	72°C	25 s
Final Extension	72°C	2 minutes
Hold	4°C	

In each PCR#1, we used a different amount of gDNA per sample to capture the full representation of the screen. For example, ~300X coverage of our genome-wide sgRNA library, gDNA from 3×10^7 cells was used, assuming 6.6 μg of gDNA for 10^6 cells, 200 μg of gDNA was used per sample (6-8 μg of gDNA per reaction). PCR#1 products for each biological sample were pooled and used for amplification with barcoded second PCR primers (see Data and code availability). For each sample, we performed at least 3 PCR#2 reactions using 2 μL of the pooled PCR#1 product per PCR#2 reactions for 10 PCR cycles. Second PCR products were pooled and gel purified from a 2% agarose gel using the MinElute Gel Extraction kit (QIAGEN). Purified product concentration was measured using a Qubit (Thermo Scientific). All products were normalized for each biological sample before combining uniquely barcoded separate biological samples. The pooled products with 10%–20% PhiX were sequenced on HiSeq 2500 system (Illumina).

Generation of artificial antigen expression lentiviral vectors

Plasmids (pCI-neo-sOVA, pCI-neo-mOVA, pCI-neo-cOVA, pcDNA3-OVA) were obtained from Addgene. Different forms of artificial tumor antigen ovalbumin sequence were subcloned into a lentiCRISPR-V2-blast vector via Gibson assembly to generate different Ova-expressing vectors (lentiV2-blast-sOva, lentiV2-blast-mOva, lentiV2-blast-cOva, lentiV2-blast-Ova).

Generation of artificial tumor antigen Ova-expressing cell lines

4T1, EMT6 and MC38 murine cancer cells were transduced with artificial tumor antigen Ova-expressing lentivirus for 24 hours. After blasticidin selection for 3 days, transduced cancer cells were cultured individually in 10 cm tissue culture plates. One week later, ovalbumin expression levels of transduced cancer cells were identified by immunoblotting.

In vivo CRISPR screening in murine cancer cells

Transduced murine cancer cells were expanded *in vitro* for 1 week to allow genome editing before being implanted into animals. Cancer cells were either injected into the mammary fat pads of mice or subcutaneously with Matrigel (1:1 dilution). Cancer cells were implanted into both flanks of 10-12 $Foxn1^{nu/nu}$ mice, 10-12 wild-type mice, 10-12 wild-type mice treated with ovalbumin, and 10-12 wild-type mice treated with ovalbumin and PD-1 blockade. Cancer cells transduced with libraries were also grown *in vitro* at approximately 1000X library coverage for the same time period as the animal experiment. Mice were vaccinated with ovalbumin twice (once a week) 14 days before cancer cell transplantation. Subsequently, mice were treated with 100 μg of rat monoclonal anti-PD-1 (clone: 29F.1A12) on days 9 and 12 via intraperitoneal injection. Mice were euthanized 16–19 days after tumor implantation and tumor genomic DNA was isolated from whole tumor tissue using a DNA extraction protocol (see above). PCR was used to amplify the sgRNA region and sequencing to determine sgRNA abundance was performed on an Illumina HiSeq. Significantly enriched or depleted sgRNAs from any comparison of conditions were identified using the MAGeCK algorithm.

Mouse validation assays

Ten thousand cancer cells (4T1, MC38) were either injected into the mammary fat pads of mice or subcutaneously with Matrigel (1:1 dilution). Tumors were measured every three days beginning on day 7 after challenge until time of death. Death was defined as the point at which a progressively growing tumor reached 2.0 cm in the longest dimension. Measurements were taken manually by collecting the longest dimension (length) and the longest perpendicular dimension (width). Tumor volume was estimated with the formula: $(L \times W^2) / 2$. CO_2 inhalation was used to euthanize mice on the day of euthanasia. Optimal group sizes were determined empirically. Researchers were not blinded to group identity and randomization of animal groups was done when appropriate.

Cell viability assays

Cancer cells were seeded in 96-well plates (500 cells per well for short time proliferation or 100 cells per well for long time proliferation), cultured 4 or 8 days before cell counting, and biologically replicated three times. For cell counting, samples were subjected to Cell Counting Kit 8 (Dojindo) following the manufacturer's protocol.

Please cite this article in press as: Wang et al., *In vivo* CRISPR screens identify the E3 ligase *Cop1* as a modulator of macrophage infiltration and cancer immunotherapy target, Cell (2021), https://doi.org/10.1016/j.cell.2021.09.006

Western blot of protein expression in murine cancer cells

Pellets from 5 × 10^6 cells were collected and digested by 500 μL RIPA Buffer (Invitrogen). Samples were incubated on ice for at least 15 minutes and centrifuged at 12,000 rpm for 10 minutes at 4°C, then subjected to BCA analysis (Thermo scientific, Cat# 23228). Approximately 40 μg of total protein from each sample was loaded for western blot analysis.

Tissue processing and flow cytometry

Tumors for flow cytometry were broken down into smaller fragments, about the size of lentils, then dissociated with 1 mg/ml Collagenase IV for 30 minutes using GentleMacs Octo Dissociator from Miltenyi, and cell suspensions were passed through 70 μm filter twice before staining. Single cancer cells were washed with ice-cold PBS with 2% FBS and stained with antibodies at 4°C for 30 minutes. Cancer cells were then washed and resuspended in ice-cold PBS with 2% FBS for flow cytometry. All data acquisition was done using an LSR II (BD) or FACS Calibur (BD Biosiences) and analyzed using FlowJo software (TreeStar) for statistical computing.

In vivo competition assays

Cancer cells were engineered to express EGFP or mCherry by lentiviral transduction to different populations. Cas9-target sgRNA-transfected cells and Cas9-control sgRNA-transfected cells were mixed and then grown for at least two passages *in vitro* before implantation into mice. Mixes were analyzed by flow cytometry on the day of tumor inoculation. Tumors were harvested and incubated in Collagenase IV for at least 30 minutes. After incubation, cancer cells were passed through 70 μm filters to remove undigested tumors. Single cancer cells were washed with ice-cold PBS with 2% FBS and stained with Near-IR Live/Dead (BD Biosciences) on ice for 30 minutes. Cancer cells were then washed and resuspended in ice-cold PBS with 2% FBS. An LSR II (BD Biosciences) was used to analyze final EGFP/mCherry cancer cell ratios.

In vitro and *in vivo* chemokine measurement

Chemokine expression levels in the culture supernatants were measured using the Mouse Cytokine Array C1000 (Raybiotech). This assay was used to quantify the concentration of chemokines secreted by cancer cells, according to the manufacturer's instructions. The results were further normalized with protein concentration of tumor cell lysates in the same experiment.

Generation of CRISPR/Cas9 Knockout cells

Construction of lenti-CRISPR/Cas9 vectors targeting Cop1 was performed following the protocol associated with the backbone vector lentiCRISPR V2 (Cat# 49535, Addgene). The sgRNA sequences used are listed in the Key resources table. 4T1 and MC38 cells were infected with lentivirus expressing sgRNAs targeting specific genes. After puromycin selection, cells were expanded and collected, and knockout was verified by western blot analyses.

RNA-seq

Total RNA was isolated and purified from the cells using Isol-RNA Lysis Reagent (Fisher) and treated with DNase I (Fisher). RNA-seq libraries were prepared using the TrueSeq Stranded Total RNA Library Prep Kit (Illumina) and sequenced on an Illumina HiSeq 2500 with 150 base paired end reads.

Real-time reverse transcription-PCR

RNA was extracted using RNeasy Plus Mini Kit (QIAGEN) from cancer cells. Then, RNA was reverse transcribed into cDNA using iScript™ cDNA Synthesis Kit (Bio-Rad Laboratories). Approximately 50 ng cDNA from each sample was mixed with gene-specific primers (Table S7) and SsoAdvanced™ universal SYBR® Green supermix (Bio-Rad Laboratories) following the manufacturer's protocol. Reactions were performed on a CFX96 Touch Real-Time PCR Detection System (Bio-Rad Laboratories).

ATAC-seq

Mouse 4T1 cells were seeded onto 6-well plates for 3 days. Each sample of 1 × 10^5 cells was trypsinized and resuspended in 50 uL cold ATAC-resuspension buffer (RSB) (10 mM Tris-HCl pH 7.4, 10 mM NaCl, and 3 mM $MgCl_2$ in water) supplemented with 0.1% NP40, 0.1% Tween-20, and 0.01% digitonin. After 3 minute incubation on ice, 1 mL ATAC-RSB containing 0.1% Tween-20 was added, and centrifuged for 10 minutes at maximum speed at 4°C. Supernatant was removed and nuclei were resuspended in 50 μL of transposition mix: 2.5 μL transposase (100 nM final), 16.5 μL 1X PBS, 0.5 μL 1% digitonin, 0.5 μL 10% Tween-20, and 5 μL water. Transposition reactions were performed at 37 °C for 30 minutes in a thermomixer, while shaking at 1000 rpm. All samples were sequenced using an Illumina HiSeq 2500 with 150 base paired end reads.

ChIP-seq

4T1 cells were plated in 15 cm tissue culture plates and cultured for 3 days. For C/ebpδ ChIP-seq, approximately 1 × 10^7 cells per condition were harvested and crosslinked by a two-step fixation, including 2 m Mdisuccinimidyl glutarate (DSG, LifeTechnologies) treatment for 45 minutes and followed by 10 minutes fixation using 1% methanol-free formaldehyde at room temperature (Eeckhoute et al., 2007; Singh et al., 2018). Cells were lysed in 1% SDS lysis buffer and sheared to 200-700 bp in size using the Covaris E220 ultrasonicator (PIP 140, DF 5%, CPB 200). Approximately 50 mg of sheared chromatin per condition were diluted and then incubated

Please cite this article in press as: Wang et al., *In vivo* CRISPR screens identify the E3 ligase *Cop1* as a modulator of macrophage infiltration and cancer immunotherapy target, Cell (2021), https://doi.org/10.1016/j.cell.2021.09.006

over night with 5 ug C/ebpδ antibody (ab245214, Abcam). Precipitates were then washed with following buffers: RIPA 0 buffer (0.1% SDS, 10 mM Tris-HCl pH 7.4, 1% Triton X-100, 1 mM EDTA, 0.1% sodium deoxycholate), RIPA 0.3 buffer (0.1% SDS, 1% Triton X-100, 0.1% sodium deoxycholate, 10 mM Tris-HCl pH 7.4, 1 mM EDTA, 0.3 M NaCl) and LiCl buffer (250 mM LiCl, 1 mM EDTA, 5% NP-40, 0.5% sodium deoxycholate, 10 mM Tris-HCl). DNA sequencing libraries were prepared using the Smarter Thruplex DNaseq kit (Takara Bio Inc.) according to the manufacturer's protocol. Libraries were sequenced on an Illumina HiSeq 2500 with 150 bp paired-end reads.

Co-immunoprecipitation

Mouse breast cancer cells were lysed in Tris buffer (50mM Tris pH 7.4, 150mM NaCl, 1mM EDTA, 0.5% NP-40, 5% glycerol, with protease and phosphatase inhibitors) for 30 minutes with gentle rocking at 4°C. Cell lysate was spun down by a centrifuge in cold room at 12,000 rpm for 10 minutes and then supernatant was collected and incubated with different antibodies coupled to Protein A/G agarose beads (Pierce Biotechnology) at 4°C overnight (12 hours). Beads were washed extensively in Tris lysis buffercontaining 0.5 M NaCl and then eluted in LDS-sample buffer (Invitrogen) containing 1% 2-mercaptoethanol. Cell lysate was supplemented with 4X SDS loading buffer (0.2 M Tris-HCl, 0.4 M DTT, 8.0% SDS, 6 mM Bromophenol blue, 4.3 M Glycerol) and heated at 95°C for 15 minutes before western blot analysis.

Single-cell RNA-seq of tumor infiltrating immune cells

Tumors grown in mice were harvested and broken down into smaller fragments, about the size of millet. Then, each sample was digested with reagents from Mouse Tumor Dissociation Kit (Miltenyi, Cat# 130-096-730) according to the manufacturer's instructions using GentleMacs Octo Dissociator from Miltenyi, and cell suspensions were passed through a 70 μm filter twice before staining. Single tumor cells were washed with ice-cold PBS containing 2% FBS and stained with CD45.2-APC/Cy7 antibody (BioLegend, Cat#109823) at 4°C for 45 minutes. All cells were then washed and resuspended in ice-cold PBS with 2% FBS. Live CD45.2 positive cells were sorted with BD Aria after staining. Each tumor from the same group was processed individually and mixed together according to the same cell number. After cell collection, immune cells were resuspended at $1x10^6$ cells/mL in PBS-0.04% BSA (Thermo Fisher Scientific, Cat# AM2616). Single cell suspensions of all samples were then barcoded with a 10x Chromium Controller (10x Genomics). RNA from the barcoded cells for each sample was subsequently reverse-transcribed and sequencing libraries were constructed with reagents from a Chromium Single Cell 30 v2 reagent kit (10x Genomics, Cat#PN-120267) according to the manufacturer's instructions. Sequencing was performed with Illumina HiSeq according to the manufacturer's instructions (Illumina).

QUANTIFICATION AND STATISTICAL ANALYSIS

Software used in this study

Cutadapt v1.8.1, Bowtie2 v2.3.3, samtools v1.9, picard v1.123, MACS2, Tophat2 v2.0.11, STAR, HT-seq v0.6.1p1, DEseq2 1.22.2, BWA, GATK, MuTect v1.1.4, ROSE v0.1, Cell Ranger v2.0.2, Seurat v2, MAGeCK v0.5.7, LISA, Cistrome-GO, clusterProfiler, deeptools, salmon, LIMMA, FastQC, and bedtools.

CRISPR screen data analysis

CRISPR data were analyzed by MAGeCK and MAGeCK-VISPR essentially as described (Chen et al., 2018a; Jeselsohn et al., 2018; Li et al., 2014). Briefly, raw sequencing data are pre-processed by using MAGeCK to obtain the read counts for each sgRNA. Control sgRNAs are used to normalize the data. MAGeCK TEST algorithm is used to compare treatment with control samples to obtain the significantly enriched and depleted sgRNAs and genes. Genes with p value less than 0.001 are candidate hits. The MaGeCKFlute package was used to visualize the data (Wang et al., 2019).

Data analysis of RNA-seq

Read alignment was performed using STAR (v2.6.1) (Dobin et al., 2013). To quantify gene expression values, we used Salmon to calculate Transcripts Per Million (TPM) and read counts using the aligned reads from STAR as input (Patro et al., 2017). Differential gene expression analysis was then performed using DESeq2 with a FDR threshold of 0.05 (Love et al., 2014). Since the *in vitro* RNA-seq was performed in two batches, the batch of the sample was considered as a covariate in DESeq2. Similarly, log-transformed TPM values were batch-effect corrected using the remove Batch Effect function in LIMMA (Ritchie et al., 2015). Gene Set Enrichment Analysis (GSEA) was performed using the clusterProfiler R package with 100,000 permutations (Yu et al., 2012).

ATAC-seq analysis

ChiLin pipeline 2.0.0 is used for QC and preprocessing of the ATAC-seq (Qin et al., 2016). We use Burrows-Wheeler Aligner (BWA) as a read mapping tool (Li and Durbin, 2009; Qin et al., 2016), and Model-based Analysis of ChIP-Seq (MACS2) as a peak caller (Zhang et al., 2008), with a q-value (FDR) threshold of 0.01. Based on a dynamic poisson distribution, MACS2 can effectively capture local biases in the genome sequence, allowing for more sensitive and robust prediction of binding sites. Unique read for 48 a position for peak calling is used to reduce false positive peaks, statically significant peaks are finally selected by calculated false discovery rate of

Please cite this article in press as: Wang et al., *In vivo* CRISPR screens identify the E3 ligase *Cop1* as a modulator of macrophage infiltration and cancer immunotherapy target, Cell (2021), https://doi.org/10.1016/j.cell.2021.09.006

reported peaks. Deeptools is used for the heatmap plots (Ramírez et al., 2016; Zhang et al., 2008). ATAC-seq Peaks from all study samples were merged to create a union set of sites. Read densities were calculated for each peak for each sample, differential peaks between WT and KO were identified by DEseq2 with adjusted $p \leq 0.05$, $|\log2\text{fold change}| \geq 1$.

Single cell RNA-seq data analysis

Cell Ranger (10x Genomics; v3.1.0) was used to align the reads to the mm10 genome and generate the count matrix with default settings. Low-quality cells containing less than 200 genes detected were removed. Genes that were present in less than 3 cells were excluded from the analysis. Seurat (v4.0.1) was used for integration (Stuart et al., 2019), normalization, dimensionality reduction, clustering, and UMAP visualization. Annotation for each cluster was performed by using MAESTRO with the "RNAAnnotateCelltype" function and "human.immune.CIBERSORT" gene signature (Wang et al., 2020). Other downstream analyses were performed with custom R (v 4.0.5) scripts.

Data analysis of ChIP-seq

The ChiLin pipeline was used to analyze Chromatin Immunoprecipitation sequencing (ChIP-seq) of C/ebpδ (Qin et al., 2016). Briefly, the bwa aligner was used to map reads to the mm10 reference genome. MACS2 (v2.1.4) was used to call ChIP-seq peaks using the command line parameters "-SPMR -B -q 0.01 –keep-dup 1" (Zhang et al., 2008). A random subsample of 4 million reads were used to assess quality control. Quality control consisted of five metrics: 1) the average read quality according to FastQC (de Sena Brandine and Smith, 2019); 2) the fraction of uniquely mapped reads; 3) a PCR bottleneck coefficient, which is the fraction of locations with one uniquely mapped read; 4) fraction of reads in peaks according to MACS2 (Zhang et al., 2008) (more, the better); 5) overlap of peaks with DNA hypersensitivity sites. All samples were of adequate quality. To provide a consistent peak set across multiple samples for downstream analysis, we merged overlapping peaks using bedtools v2.29.2 (Quinlan and Hall, 2010). Differential peak analysis between *Rosa26* and Cop1 KO was then performed using DESeq2 with a False Discovery Rate threshold of 0.05 and $|\log2FC| > 0.5$ (Love et al., 2014). A heatmap visualizing the peaks was then generated using the deeptools package (v3.3.0) (Ramírez et al., 2016). KEGG pathway enrichment of the upregulated C/ebpδ peaks was then conducted using Cistrome GO (Li et al., 2019).

Cop1 degron motif prioritization

Cop1 Degron Motif Search

A degron sequence motif for Cop1 was downloaded from the Eukaryotic Linear Motif Database (Gouw et al., 2018), which was represented by the regular expression "[STDE]{1,3}.{0,2}[TSDE].{2,3}VP[STDE]G{0,1}[FLIMVYPA]." Protein sequences from the mouse and human proteome were downloaded (10/2/2019) from the Swiss-Prot reviewed sequences of the UniProt database (UniProt Consortium, 2019) . The Cop1 degron sequence motif was then searched against Swiss-Prot sequences using the python "re" package. This resulted in 1,196 hits (1,067 genes) in mice and 1,328 (1,010 genes) in humans.

Machine learning prioritization

Not all instances of a sequence motif may be a biologically plausible degron. To further refine plausible candidates, we developed a model to predict the potential of a motif to be a degron. A Random Forest algorithm was trained (number of trees = 1,000) on 83 features from the SNVBox database (UniProt Consortium, 2019; Wong et al., 2011) to distinguish previously reported degrons (n = 186) (Mészáros et al., 2017) from random other sequences within the same set of proteins (n = 186). Features spanned characterization of evolutionary conservation to biophysical features of amino acid residues within a protein. To summarize features across the multiple amino acid residues in a motif, we took the average of each feature. Evaluated using 20-fold cross-validation, performance as measured by the area under the Receiver Operating Characteristic curve (auROC) was 0.81 out of 1.0 ($p = 2 \times 10^{-25}$, Mann-Whitney U test).

Cop1 Degron Motif Filtering

Given the large number of motif hits found in mice, we filtered out those not also seen in humans or which had low degron potential according to machine learning predictions. Of the 1,067 genes with motif hits in mice, 448 showed overlap in humans. After filtering for a high Random Forest score (> 0.5 out of 1.0), 117 high-scoring motifs remained. Among the high scoring candidates, numerous were for previously reported Cop1 substrates, such as Ets1, Etv5 and Jun (Marine, 2012).

Gene signature analysis

Cop1 gene expression signature

We created an RNA expression gene signature for Cop1 KO based on the top 500 differentially expressed genes (250 upregulated, 250 downregulated). Genes within the signature were weighted by their log2 fold change values reported by DESeq2 in the Cop1 KO versus *Rosa26*

(control) condition without IFNG treatment. Only mouse genes with a corresponding human gene were used. A Cop1 signature score was computed by a weighted linear combination of Cop1 KO log2 fold changes with normalized expression values from TCGA (see below).

Please cite this article in press as: Wang et al., *In vivo* CRISPR screens identify the E3 ligase *Cop1* as a modulator of macrophage infiltration and cancer immunotherapy target, Cell (2021), https://doi.org/10.1016/j.cell.2021.09.006

TCGA expression data

RSEM quantifications (v2) for RNA expression data from The Cancer Genome Atlas (TCGA) was downloaded from the genomic data commons (https://portal.gdc.cancer.gov/). RNA expression was then log2 normalized, followed by subtracting the median expression value for each gene across the cohort.

Correlation with Immune Cell Infiltration

Immune cell infiltration was inferred from bulk RNA-seq data using the immunedeconv R package (Sturm et al., 2019), which contains estimates based on 6 different methods (CIBERSORT (absolute mode), TIMER, xCell, EPIC, MCP-counter, quanTIseq) (Aran et al., 2017; Becht et al., 2016; Finotello et al., 2019; Li et al., 2016; Newman et al., 2015; Racle et al., 2017). Cop1 signature scores were then analyzed for their correlation with immune cell infiltration estimates, after adjusting for tumor purity (partial spearman correlation, see (Li et al., 2017)). Benjamini-Hochberg correction was then applied across all p values and a correlation was deemed significant at a FDR < 0.05.

Cytokine and surface receptor/ligand genes

To analyze genes that may impact the tumor-immune microenvironment, we curated a set of cytokine and surface receptor related genes: ''Cytokine-Cytokine Receptor Interaction'' pathway from KEGG database and surface receptor/ligand genes as reported previously (Kanehisa and Goto, 2000; Ramilowski et al., 2015).

CellPress

Supplemental figures

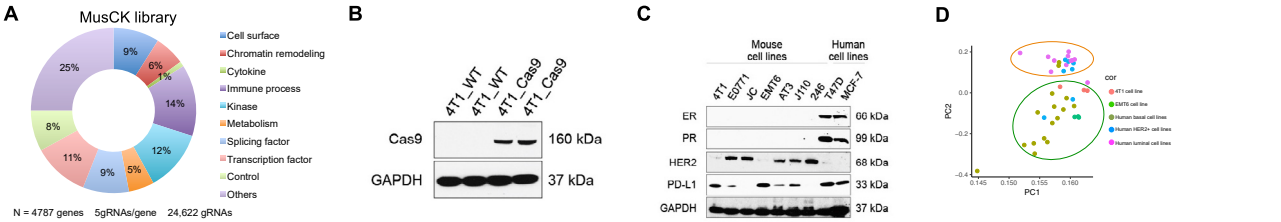

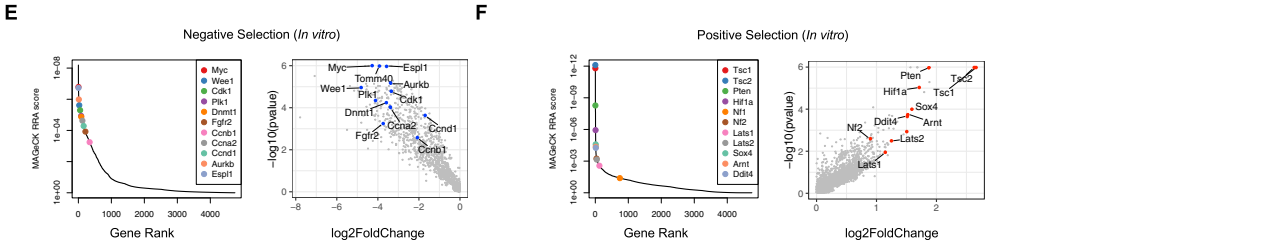

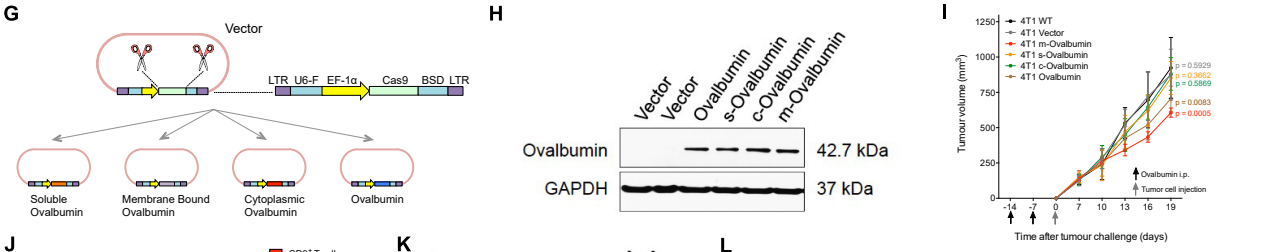

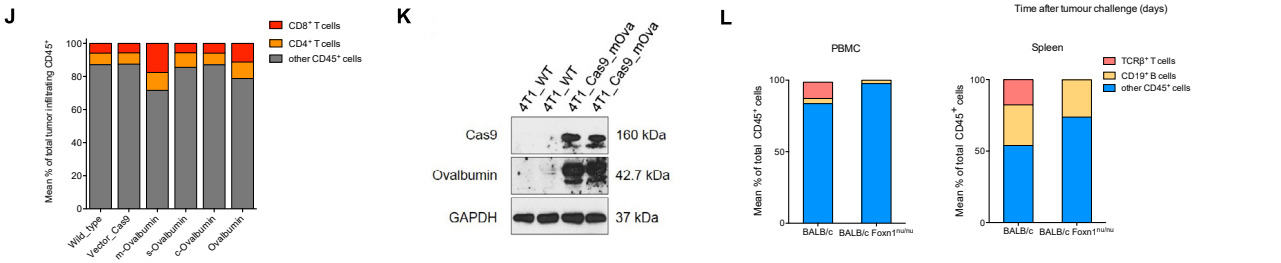

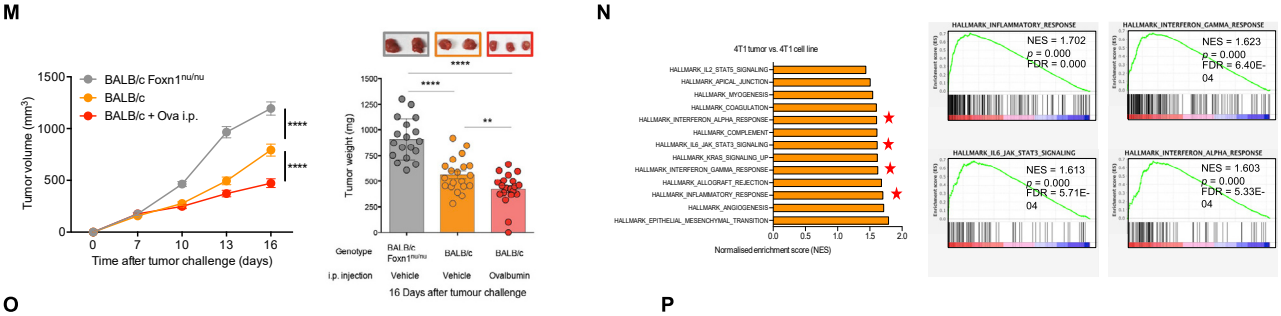

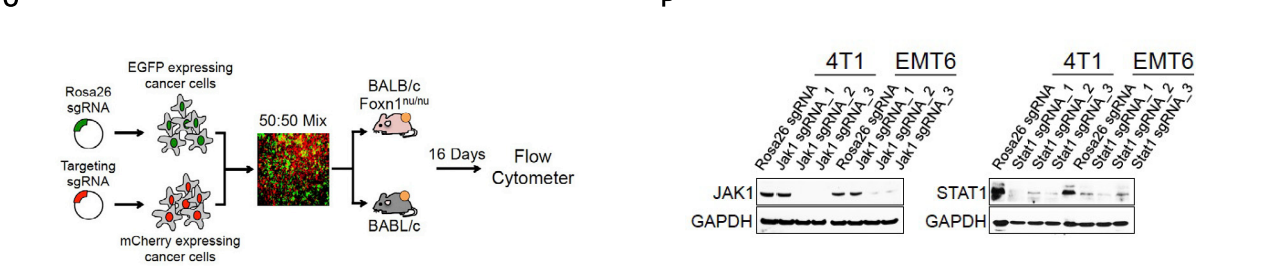

(legend on next page)

Figure S1. Optimization and validation of primary MusCK *in vivo* CRISPR screens in the mouse 4T1 TNBC models, related to Figure 1

(A) Pie chart showing the fraction of genes targeted in the MusCK library.
(B) Protein Cas9 expression in MusCK library-infected 4T1 cells.
(C) Expression of hormone receptors and PD-L1 in mouse and human cancer cells.
(D) Principal component analysis of transcriptome of mouse and human breast cancer cells.
(E) MAGeCK analysis and RRA ranking of top depleted genes in the *in vitro* MusCK screen.
(F) MAGeCK analysis and RRA ranking of top enriched genes in the *in vitro* MusCK screen.
(G) Mouse 4T1 cell line was transduced with a vector expressing various forms of ovalbumin antigen.
(H) western blot of 4T1 cell lysate for ovalbumin and GAPDH after transfection with either control or ovalbumin vector.
(I) Tumor volume of wild-type or ovalbumin expressing 4T1 cancers.
(J) Tumor infiltrating T cells in wild-type or ovalbumin expressing 4T1 cancers.
(K) western blot of 4T1 cell lysate for Cas9, ovalbumin and GAPDH after transduction with CRISPR library.
(L) Flow cytometry analysis of T cells and B cells in different host conditions.
(M) Tumor volume averaged for groups indicated and tumor weight measured at 16 days post implantation. n = 12 per group.
(N) Gene set enrichment analysis of 4T1 tumor and 4T1 cells. Top enriched pathways in 4T1 tumors versus 4T1 cells were shown. GSEA terms significantly upregulated in 4T1 tumors compared with 4T1 cells.
(O) Scheme of *in vivo* competition between *Jak1* or *Stat1* KO and control *Rosa26* KO cells.
(P) western blotting of *Jak1* and *Stat1* expression in 4T1 and EMT6 cells transduced with single gRNA targeting *Jak1 (*or *Stat1)*.

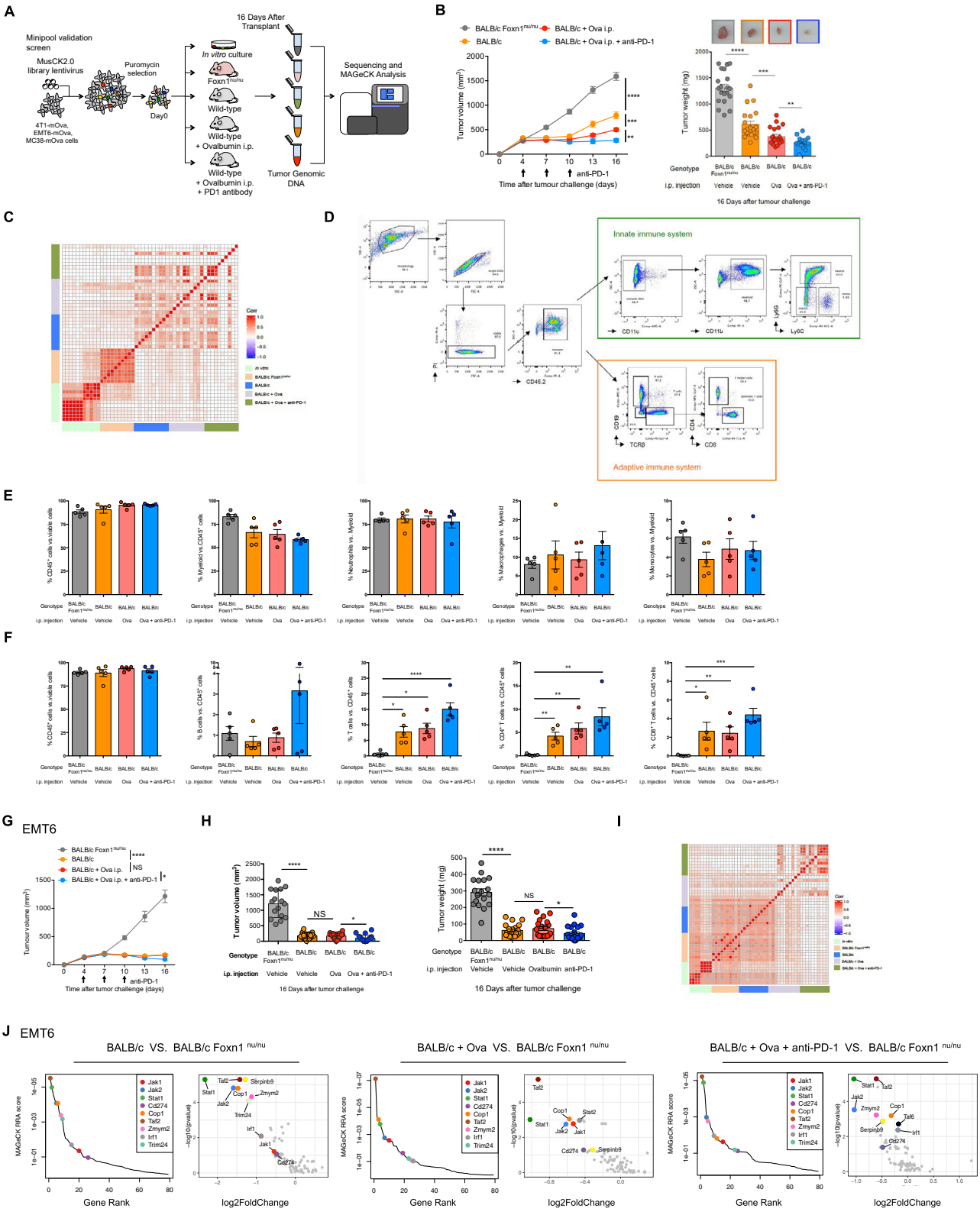

(legend on next page)

Figure S2. MusCK 2.0 library screens on 4T1 and EMT6 TNBC mouse models, related to Figure 2

(A) Scheme of MusCK 2.0 *in vivo* screen.

(B) Tumor volume of 4T1 tumor averaged for groups indicated and tumor weight measured at 16 days post implantation. Error bars represent ± 1 SEM, n = 10 mice per group.

(C) A matrix of the Pearson's correlations of the library distribution from one animal compared to any other animal for MusCK 2.0 screen using 4T1 cells.

(D) Representative plots showing the gating strategy for different populations of tumor infiltrating immune cells.

(E and F) Flow cytometry analysis of tumor infiltrating immune cell population in mice under different treatment. Data are shown as mean ± SEM, n = 5 per group, *p < 0.05, **p < 0.01, ***p < 0.001, ****p < 0.0001, by one-way ANOVA with Benjamini-Hochberg post-test multiple comparison.

(G) Tumor volume of EMT6 tumor averaged for groups indicated. Error bars represent ± 1 SEM, n = 10-12 mice per group.

(H) EMT6 tumor volume and weight measured at 16 days post implantation. Data are shown as mean ± SEM, n = 10-12 mice per group, *p < 0.05, ****p < 0.0001, by one-way ANOVA with Benjamini-Hochberg post-test multiple comparison.

(I) A matrix of the Pearson's correlations of the library distribution from one animal compared to any other animal for MusCK 2.0 screen using EMT6 cells.

(J) MAGeCK analysis and RRA ranking of top depleted genes in the MusCK 2.0 screen.

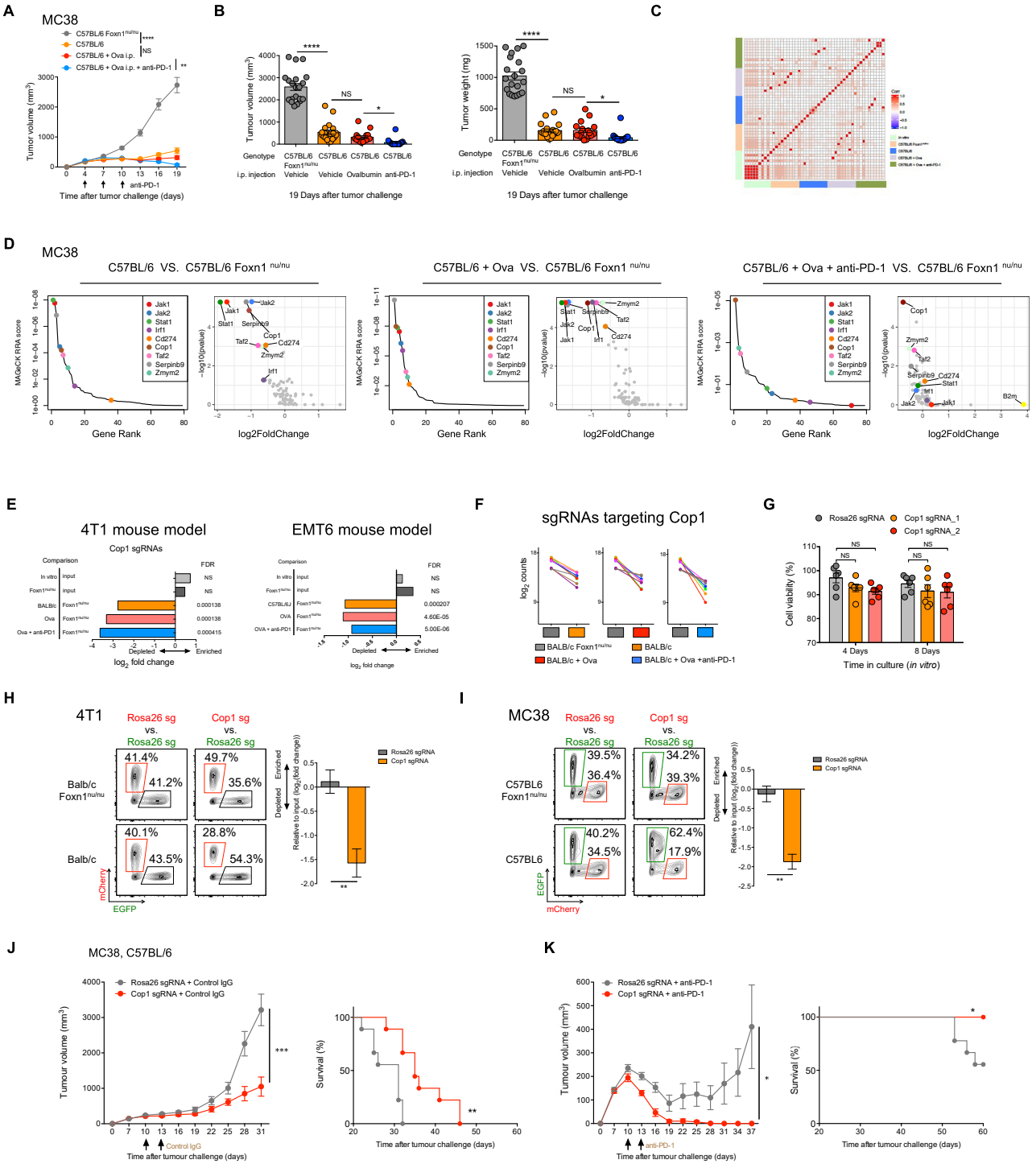

Figure S3. MusCK 2.0 library screens on MC38 colon cancer mouse models and identification of *Cop1* function on mouse models, related to Figure 2

(A) Tumor volume of MC38 tumor averaged for groups indicated. Error bars represent ± 1 SEM, n = 10-12 mice per group.

(B) Tumor volume and weight measured at 19 days post implantation. Data are shown as mean ± SEM, n = 10-12 mice per group, *p < 0.05, ****p < 0.0001, by one-way ANOVA with Benjamini-Hochberg post-test multiple comparison.

(C) A matrix of the Pearson's correlations of the library distribution from one animal compared to any other animal for MusCK 2.0 screen using MC38 cells.

(D) MAGeCK analysis and RRA ranking of top depleted genes in the MusCK 2.0 screen.

(E) Frequency of sgRNAs targeting *Cop1* in the MusCK 2.0 screen on 4T1 and EMT6 TNBC mouse models.

(legend continued on next page)

(F) Behavior of individual sgRNAs targeting *Cop1* in MusCK 2.0 screen in 4T1 TNBC models.
(G) Cell viability of *Rosa26* and *Cop1* KO 4T1 cells cultured *in vitro*. Data are shown as mean ± SEM, n = 6 per group, by one-way ANOVA with Benjamini-Hochberg post-test multiple comparison.
(H) Flow cytometry analysis of *Cop1* KO cells versus control cells in the resulting 4T1 tumors.
(I) Flow cytometry analysis of *Cop1* KO cells versus control cells in the resulting MC38 tumors.
(J and K) Tumor volume and Kaplan-Meier survival analysis of host animals bearing *Rosa26* and *Cop1* KO MC38 tumors under immunoglobulin G (IgG) isotype or anti-PD-1 antibody treatment. Data are shown as mean ± SEM, n = 10 mice per group, *$p < 0.05$, ***$p < 0.001$, by one-way ANOVA with Benjamini-Hochberg post-test multiple comparison.

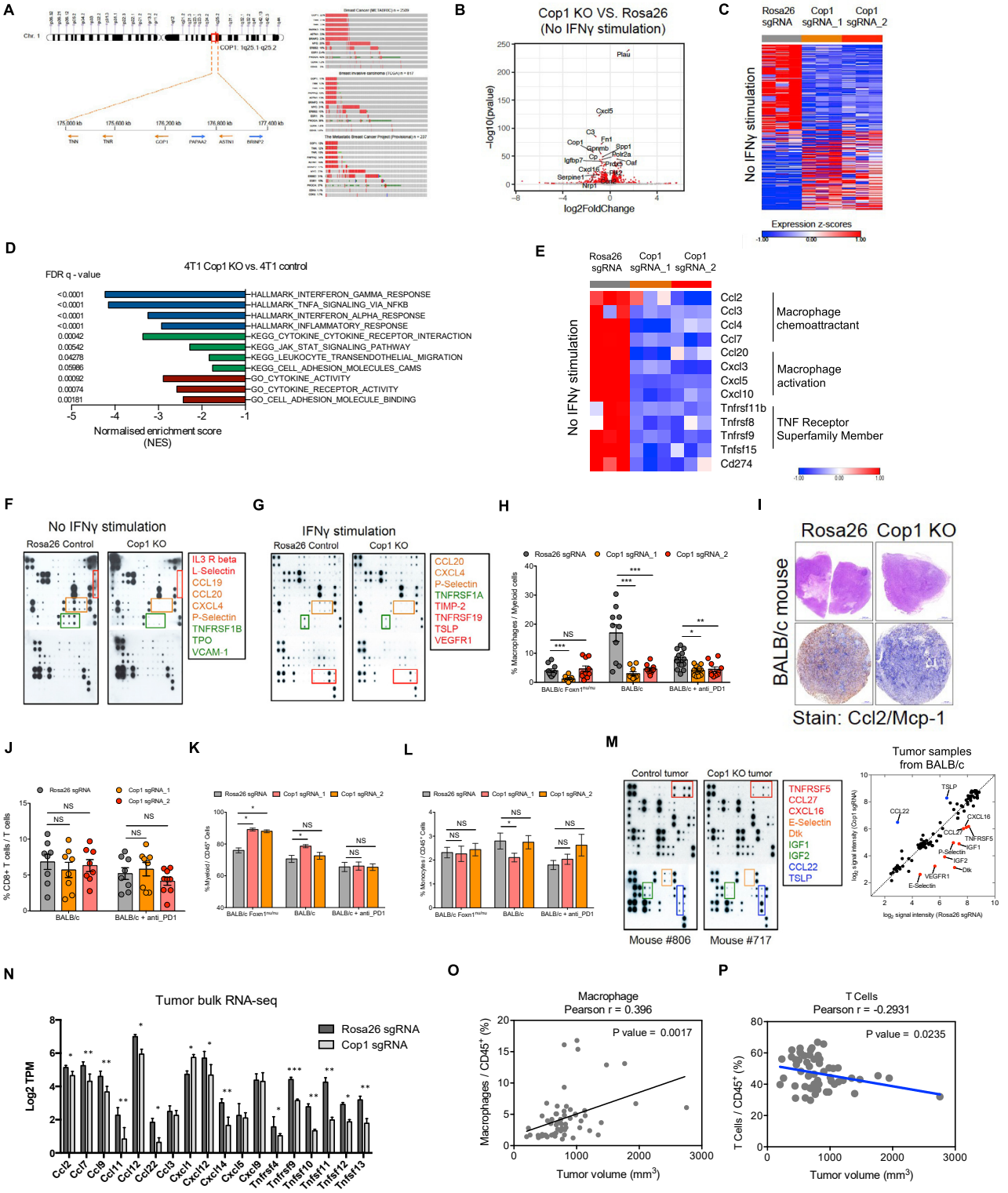

Figure S4. *Cop1* KO sensitized cancer cells to immune-mediated cytotoxicity, related to Figure 3

(A) Location of *COP1* (*RFWD2*) gene on chromosome 1 and percentage of subjects with *COP1* gene amplification (red) in different breast cancer datasets.

(B) RNA-sequencing of *Rosa26* and *Cop1* KO 4T1 cancer cells without IFNγ stimulation. Red dots denote genes significantly ($p < 0.05$) differentially expressed in conditions compared.

(legend continued on next page)

(C) Heatmap showing differential transcriptomic expression in *Rosa26* and *Cop1* KO 4T1 cells without IFNγ stimulation.
(D) Gene set enrichment analysis of *Rosa26* and *Cop1* KO 4T1 cancer cells without IFNγ stimulation. Top depleted pathways in *Cop1* KO cells versus *Rosa26* control cells were shown.
(E) Differential transcriptomic expression of macrophage-related genes in *Rosa26* and *Cop1* KO 4T1 cells without IFNγ stimulation.
(F) Representative images of chemokines from proteome array analysis of control (*Rosa26*) and *Cop1* KO 4T1 *in vitro* cell culture supernatants without IFNγ stimulation.
(G) Representative images of chemokines from proteome array analysis of control (*Rosa26*) and *Cop1* KO 4T1 *in vitro* cell culture supernatants with IFNγ stimulation.
(H) Quantification of percentage of macrophages in all tumor-infiltrating myeloid cells. Data are shown as mean ± SEM, n = 8-10 per group, $*p < 0.05$, $**p < 0.01$, $***p < 0.001$, by one-way ANOVA with Benjamini-Hochberg post-test multiple comparison.
(I) Immunohistochemistry of sections showing monocyte chemoattractant CCL2/MCP1 expression in *Rosa26* and *Cop1* KO 4T1 tumors.
(J) Flow cytometry analysis of $CD8^+$ T cell populations in *Rosa26* and *Cop1* KO 4T1 tumors grown in BALB/c mice under different treatment *in vivo*. Quantification of percentage of $CD8^+$ T cells in all tumor-infiltrating T cells.
(K) Flow cytometry analysis of myeloid cell populations in *Rosa26* and *Cop1* KO 4T1 tumors grown in BALB/c mice under different treatment *in vivo*. Quantification of percentage of myeloid cells in all tumor-infiltrating $CD45^+$ cells.
(L) Flow cytometry analysis of monocyte populations in *Rosa26* and *Cop1* KO 4T1 tumors grown in BALB/c mice under different treatment *in vivo*. Quantification of percentage of monocytes in all tumor-infiltrating $CD45^+$ cells.
(M) Representative images of chemokines from proteome array analysis of control (*Rosa26*) and *Cop1* KO 4T1 tumors (left). Quantification of differential protein expression (in cytokine array) of tumor extracts harvested from host animals (right).
(N) Gene expressions of macrophage-associated chemokines and chemokine receptors of control (*Rosa26*) and *Cop1* KO 4T1 tumors grown in BALB/c hosts.
(O) Correlation of macrophage infiltration with tumor volume at end point.
(P) Correlation of T cell infiltration with tumor volume at end point.

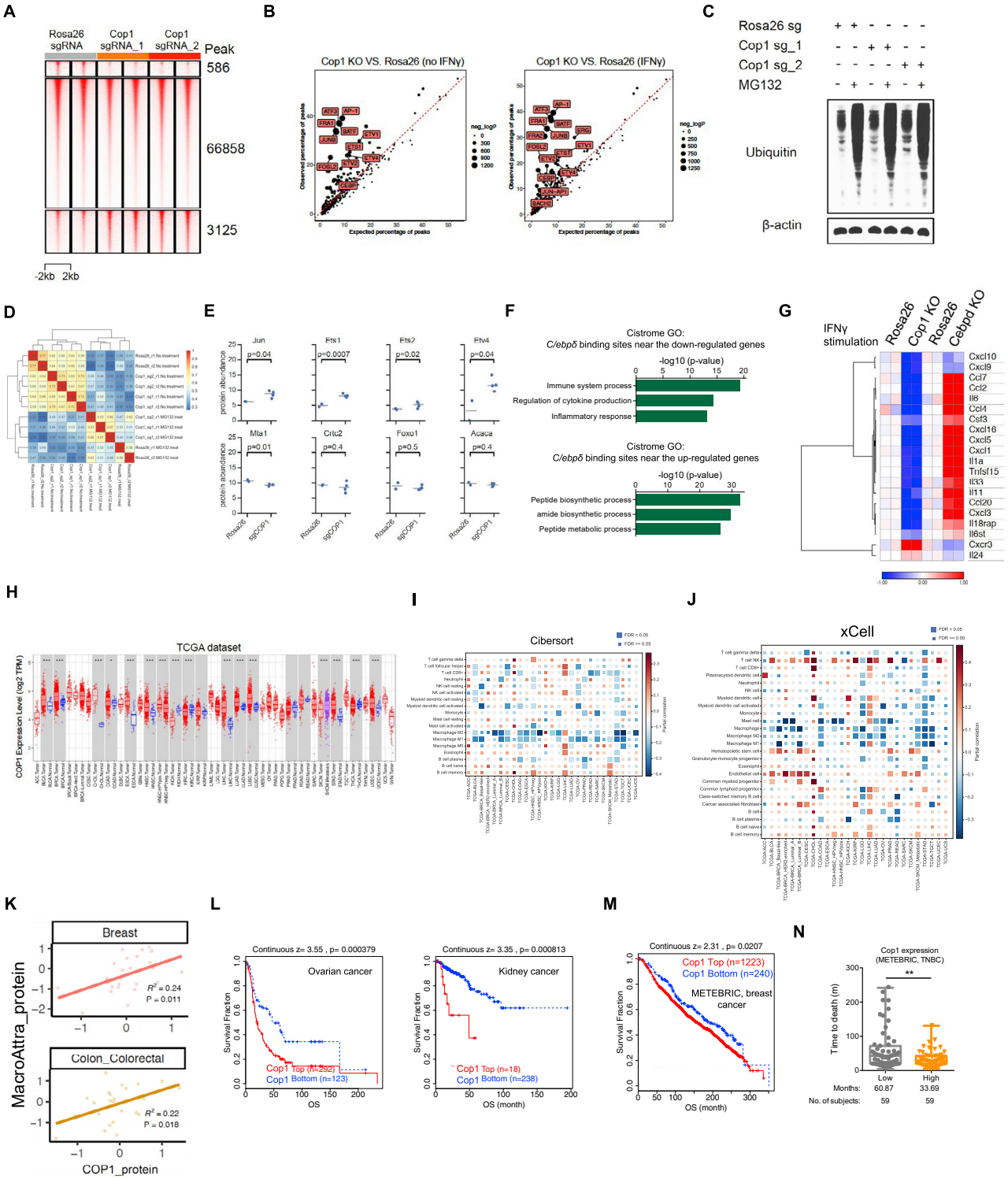

Figure S5. Prioritization of putative *Cop1* substrates, related to Figures 4 and 5

(A) Heatmap showing changes in chromatin accessibility of *Rosa26* and *Cop1* KO 4T1 cancer cells without IFNγ stimulation.

(B) TF motif enrichment of *Rosa26* and *Cop1* KO 4T1 cancer cells with or without IFNγ stimulation. Expected (x axis) versus observed (y axis) percentages of IFNγ treated cells peaks overlapping each TF binding site annotation.

(C) western blot of protein ubiquitination levels in *Rosa26* KO and *Cop1* KO 4T1 cells under treatment of vehicle or MG132 (at 50 μM for 8 hours).

(D) Heatmap displaying the correlation in the proteome for samples indicates consistency among replicates. Color indicates the spearman correlation.

(legend continued on next page)

(E) Differential protein abundance (*Cop1* KO VS. *Rosa26* 4T1 cells) of previously reported substrates of *Cop1*.
(F) Significant enriched ontology terms of *Cop1* KO-specific *C/ebpδ* peaks. p values determined by hypergeometric test.
(G) Heatmap showing differential transcriptomic expression in *Rosa26* KO and *C/ebpδ* KO 4T1 cells with IFNγ stimulation.
(H) Compared to adjacent normal tissue, *COP1* was overexpressed in TCGA cancer samples. Data are shown as mean ± SEM, *p < 0.05, ***p < 0.001, by Mann-Whitney U test.
(I and J) Partial spearman correlation after adjusting for tumor purity of the *Cop1* gene expression signature with estimated immune cell infiltration of tumors from I) Cibersort, and J) xCell. x axis reflects cancer types from TCGA and y axis is immune cell types.
(K) Correlation of *COP1* protein level with protein levels of macrophage-associated chemokines, upon *Cop1* KO in multiple human breast and colorectal cancer cell lines.
(L) Kaplan-Meier plot displaying that higher *COP1* expression associates with worse survival in the ovarian and kidney cancer cohorts (Cox PH test).
(M and N) Kaplan-Meier plot displaying that higher *COP1* expression associates with worse survival in the METABRIC breast cancer cohort (Cox PH test). The association with survival was still significant when restricting Triple Negative Breast Cancer (TNBC) (Mann-Whitney U test).

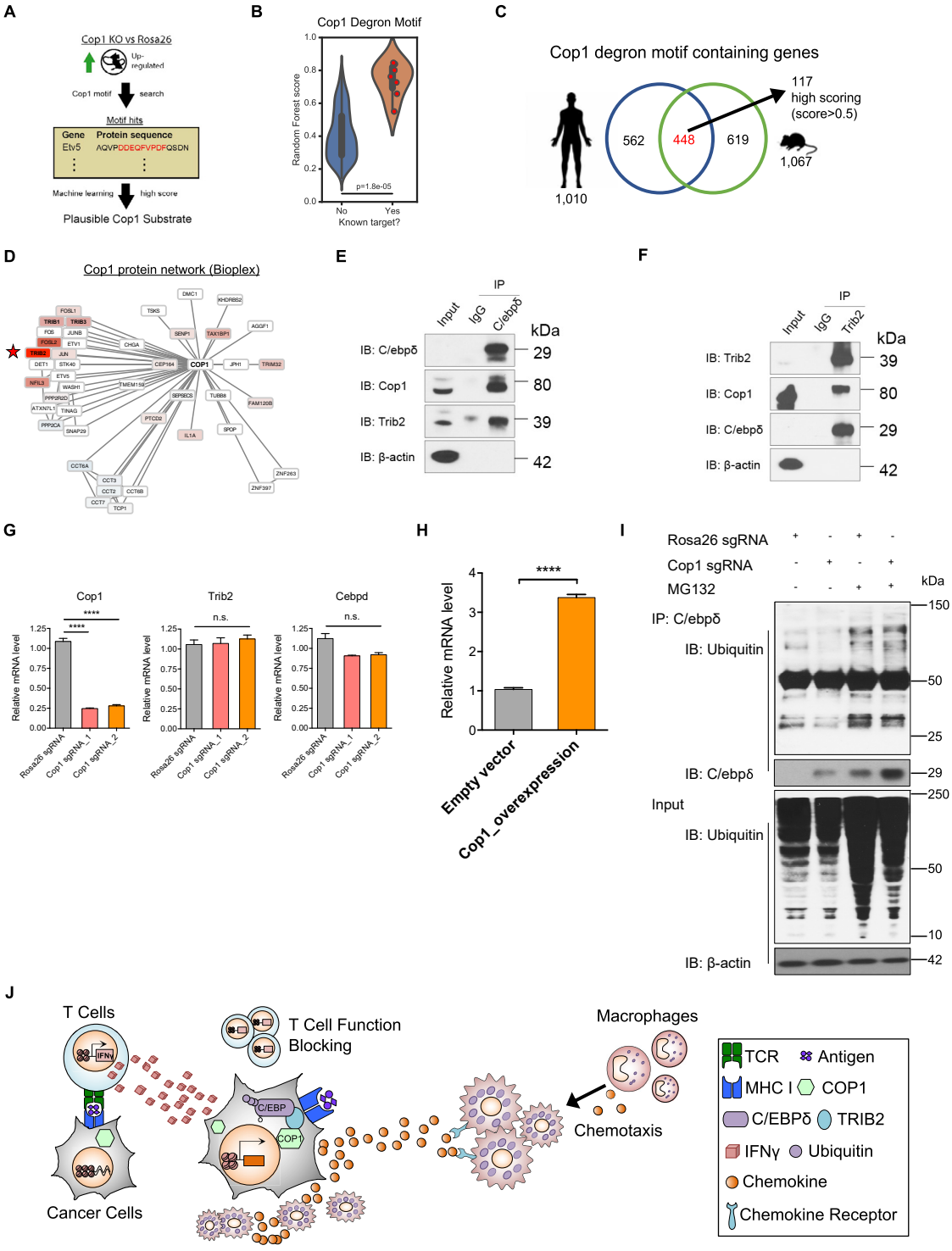

Figure S6. *Trib2* serves as a substrate adaptor for *Cop1* to target *C/ebpδ*, related to Figure 6

(A) Diagram displaying that putative *Cop1* substrates must be upregulated at the protein-level upon *Cop1* KO, contain a *Cop1* degron motif, and score well according to a machine learning model.

(B) Scoring of the degron-likelihood by the RF algorithm of *Cop1* motifs indicates known *Cop1* substrates received higher scores. Boxplot represents quartiles ± 1.5 interquartile range. Mann-Whitney U test.

(C) Overlapping the results from mouse and human showed 117 motif hits as possible *Cop1* degrons (score > 0.5).

(legend continued on next page)

(D) Protein interaction network of human *COP1* (Bioplex database) indicates tribbles protein family (TRIB1/2/3) physically interact with *COP1*. Colors denote differential expression upon *Cop1* KO: red = upregulated, blue = downregulated.
(E and F) The lysate from wild-type 4T1 cells were incubated with *Trib2* and *C/ebpδ* antibody or normal control IgG, and the immunocomplexes were probed with the indicated antibodies.
(G) Relative mRNA levels of *Cop1*, Trib2 and *C/ebpδ* in *Rosa26* KO and *Cop1* KO cancer cells. Data are shown as mean ± SEM, 3 replicates per condition, ****$p < 0.0001$, by one-way ANOVA with Benjamini-Hochberg multiple test correction.
(H) Real time PCR analysis confirmed that the *Cop1* overexpression condition was indeed overexpressed compared to the empty vector.
(I) western blot of protein ubiquitination levels of *Rosa26* KO and *Cop1* KO 4T1 cells under treatment of vehicle or MG132.
(J) Model for *Cop1*-driven macrophage infiltration.